Journal of Physiology (1993), **466**, *pp.* 9–37
With 13 *figures*
Printed in Great Britain

KINETIC ANALYSIS OF TWO TYPES OF Na^+ CHANNELS IN RAT DORSAL ROOT GANGLIA

BY NOBUKUNI OGATA AND HIDEHARU TATEBAYASHI

From the Department of Pharmacology, Faculty of Medicine, Kyushu University, Fukuoka 812, Japan

(*Received 25 July 1992*)

SUMMARY

1. The gating properties of two types of Na^+ channels were studied in neurones isolated from rat dorsal root ganglia using the whole cell variation of the patch electrode voltage-clamp technique.

2. Two types of Na^+ currents (I_{Na}) were identified on the basis of their sensitivity to tetrodotoxin (TTX). One type was insensitive to TTX (up to 0·1 mM), while the other type was blocked by 1 nM of TTX. Whereas they were both insensitive to 50 μM Cd^{2+}, a high concentration (2 mM) of Co^{2+} selectively inhibited the TTX-insensitive type.

3. The activation thresholds were about -60 and -40 mV for the TTX-sensitive and the TTX-insensitive I_{Na}, respectively. Activation of the TTX-sensitive I_{Na} developed with a sigmoidal time course which was described by m^3 kinetics, whereas the activation of the TTX-insensitive I_{Na} was described by a single exponential function. A deactivation process, as measured by the tail current upon repolarization, followed an exponential decay in either type of I_{Na}.

4. The rate constant of activation indicated that under comparable membrane potential conditions, the TTX-insensitive channels open 4–5 times slower than the TTX-sensitive ones upon depolarization. Likewise, the rate constant of inactivation indicated that the TTX-insensitive channels inactivate 3–7 times more slowly than the TTX-sensitive ones upon repolarization.

5. The steady-state activation curve for the TTX-insensitive I_{Na} was shifted about 20 mV in the positive direction from that for the TTX-sensitive I_{Na}.

6. The steady-state inactivation curve for the TTX-insensitive I_{Na} as obtained with a 0·5 s prepulse was shifted about 26 mV in the positive direction from that for the TTX-sensitive I_{Na}, indicating a greater availability for the TTX-insensitive I_{Na} in depolarized membrane. However, on increasing the duration of prepulse, the inactivation curve for the TTX-insensitive I_{Na}, but not for the TTX-sensitive I_{Na}, shifted in the negative direction due to an extremely slow inactivation process in the TTX-insensitive I_{Na}. Consequently, an overlap between the activation and inactivation curves which causes a steady influx of Na^+ (window current) became progressively reduced.

7. The time course of I_{Na} decay was best described by a single exponential process in either the TTX-sensitive or TTX-insensitive I_{Na}, whereas the development of

inactivation and the recovery from inactivation, which were measured by a conventional double-pulse protocol, followed a second order process in either channel type.

8. It was concluded that the two types of Na^+ channels have remarkably different gating mechanisms. These two types of Na^+ channels observed in sensory neurones may contribute to the encoding of different types of sensations in the sensory signal processing.

INTRODUCTION

Neurones in the dorsal root ganglia (DRG) are composed of two major classes on the basis of their morphological and histological features, the large light cells and the small dark cells (Lawson, Harper, Harper, Garson & Anderton, 1984). The peripheral C fibres originate from neurones in the size range of the small dark cell population, whereas the peripheral Aα and Aβ fibres originate from neurones in the size range of the large light cell population (Harper & Lawson, 1985*a*; Lee, Chung, Chung & Coggeshall, 1986), indicating that the two types of neurones play different functional roles in sensory integration.

Action potentials in mammalian DRG neurones are partially resistant to tetrodotoxin (TTX) (Yoshida, Matsuda & Samejima, 1978; Fukuda & Kameyama, 1980). TTX-insensitive Na^+ currents (I_{Na}) have been shown in DRG (Kostyuk, Veselovsky & Tsyndrenko, 1981) and cranial sensory (nodose ganglion) neurones (Bossu & Feltz, 1984; Ikeda & Schofield, 1987; Ikeda, Schofield & Weight, 1986). The TTX-insensitive I_{Na} can be recorded not only in immature (day 17 of gestation) neurones but also in adult neurones (Ogata & Tatebayashi, 1992*a*), suggesting that the TTX-insensitive Na^+ channels are not only transiently expressed during early stages of development but may be permanently expressed for developed neuronal functions. We have recently shown that the TTX-sensitive neurone and the TTX-insensitive neurone are closely correlated in their size distributions with the large light cell and the small dark cell, respectively (Ogata & Tatebayashi, 1992*a*). Thus, the two types of Na^+ channels appear to play important roles in sensory integration.

In addition to sensory neurones, the TTX-insensitive I_{Na} has been found in other peripheral neurones such as the rat superior cervical neurone (Schofield & Ikeda, 1988), the bull-frog parasympathetic neurone (Clark, Tse & Giles, 1990) and the rat parasympathetic neurone (Groat, Weight & White, 1989). Therefore, it is suggested that the TTX-insensitive Na^+ channel may be widespread in the peripheral nervous system and involved in a variety of cellular functions. Thus, detailed knowledge of the gating property of TTX-insensitive Na^+ channels, in addition to those of the well-established TTX-sensitive ones, would be indispensable for understanding the processing of sensory signals. We report here the gating kinetics of the TTX-sensitive and TTX-insensitive Na^+ channels in cultured neurones obtained from newborn rat DRG.

METHODS

Dissociation and culture procedures

Procedures for dissociation and culture of neurones in the dorsal root ganglia (DRG) were as described previously (Tatebayashi & Ogata, 1992). Newborn rats (1–2 days postnatal) were killed by decapitation under ethylether anaesthesia. The DRGs were dissected out and incubated at 36 °C

for 30–40 min in Ca^{2+}- and Mg^{2+}-free saline, containing 0·25% trypsin (Type XI, Sigma, St Louis, MO, USA). The ganglia were then mechanically dissociated with a fire-polished Pasteur pipette. Dissociated cells were kept in the Krebs solution at room temperature (21–23 °C). The Krebs solution contained (mM): 120 NaCl, 5 KCl, 1·8 $CaCl_2$, 1 $MgCl_2$, 5 Hepes and 25 glucose (pH 7·4). The cells were plated on glass cover-slips coated with poly-L-lysine (Sigma) and maintained in a humidified incubator containing 5% CO_2 in air at 35 °C in Dulbecco's modified Eagle's medium supplemented with 10% fetal bovine serum (GIBCO), penicillin (40 i.u./ml), and streptomycin (40 ng/ml). After 1–2 days in culture, cytosine β-D-arabinofuranoside (Sigma) was added to cultures to suppress the growth of non-neuronal cells. Subsequent medium changes were made at 3–4 day intervals. Cells were used between 3 and 4 weeks in culture.

Electrical recording

The methods for electrical recording used in the present study were similar to those previously described (Ogata, Yoshii & Narahashi, 1990). Membrane currents were recorded with the whole-cell patch-clamp technique (Hamill, Marty, Neher, Sakmann & Sigworth, 1981). The DC resistance of suction electrodes was 0·5–0·8 MΩ. Two types of pipette solutions were used in the preliminary experiments. One solution contained (mM): 120 caesium glutamate, 10 NaCl, 2·5 $MgCl_2$, 5 glucose, 5 Hepes, and 5 EGTA. The other solution contained (mM): 135 CsF, 10 NaF, 5 Hepes. These two types of internal solutions produced the same results in recordings of I_{Na}. However, an addition of polyvalent cation Ca^{2+} channel blockers was required to suppress the Ca^{2+} currents in the former solution. To avoid a possible indirect effect due to surface charge of polyvalent cations (see Results), the latter solution was used in the present study. The pH of the pipette solution was adjusted to 7·0 with CsOH.

The external solution contained (mM): 100 NaCl, 5 CsCl, 1·8 $CaCl_2$, 1 $MgCl_2$, 5 Hepes, 20 tetraethylammonium chloride, 25 glucose. In some experiments, HCO_3^- buffer was used under continuous CO_2 bubbling instead of Hepes buffer. Since we did not find any detectable difference in sodium current recordings between two buffer systems, Hepes buffer was used throughout the experiments. The pH of the external solution was adjusted to 7·4 with NaOH. In some experiments, the total amount of external NaCl was replaced with an equimolar amount of tetramethylammonium chloride.

All the experiments were performed with an on-line system which has been developed by M. Yoshii and N. Ogata, using a personal computer (PC-286V, Epson, Tokyo, Japan). Membrane currents passing through the pipette were recorded by a current-to-voltage converter designed by M. Yoshii (Narahashi, Tsunoo & Yoshii, 1987) and stored on hard disk. Compensation for series resistance was performed by adding a part of the output voltage of the current recording to the command pulse. Capacitative and leakage currents were subtracted digitally by the P-P/4 procedure (Ogata *et al.* 1990). In addition, the TTX-sensitive component of I_{Na} was obtained by subtracting the current remaining after application of 1 μm TTX from the total I_{Na}. The liquid-junction potential between internal and external solutions was about 11 mV. The data shown here were compensated for this effect by adjusting the zero-current potential to the liquid-junction potential. Only cells showing an adequate voltage and space clamp (Ogata, Nishimura & Narahashi, 1989) were used. The baseline of current at the holding potential was continuously recorded with an ink writer. After an initial stabilization period of about 15 min, experiments were started. Programmed sequences of voltage pulses were applied to the preparation from the computer using a digital-to-analog converter.

Experiments were performed at room temperature (21–23 °C). Drugs were applied through a rapid microsuperfusion system (Ogata & Tatebayashi, 1991). Results are expressed as means ± S.E.M., and n represents the number of cells. Exponential fits were determined by computer using a non-linear sum of the least squares fitting routine.

RESULTS

TTX sensitivity of I_{Na}

Neurones in the rat DRG could be divided into three groups according to their responsiveness to TTX (Fig. 1*A*). The first group was characterized by I_{Na} which was totally suppressed by a low concentration (1 nM) of TTX (TTX-sensitive cells, *Aa*). The second group had I_{Na} which was insensitive to TTX (TTX-insensitive cells, *Ab*).

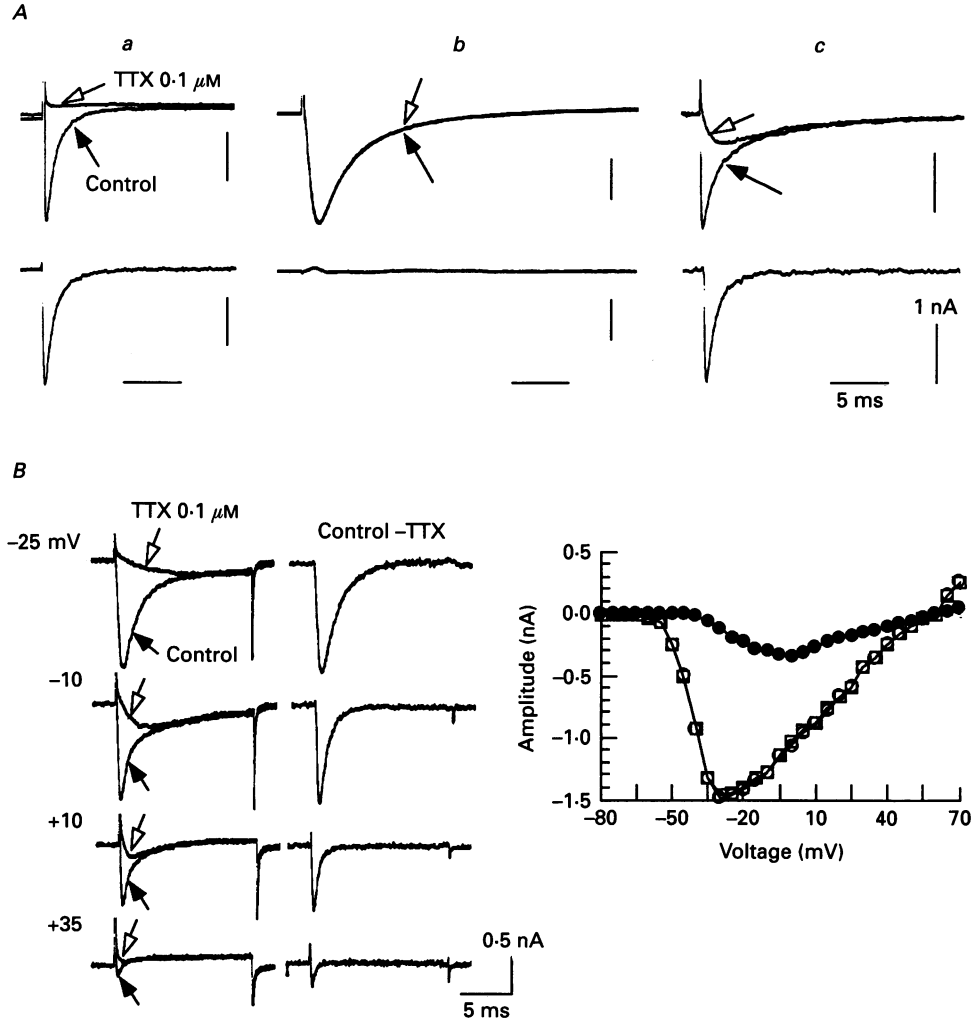

Fig. 1. Two types of Na^+ channels in rat DRG neurones. *A*, Na^+ current (I_{Na}) was evoked by 30 ms voltage steps to −10 mV from a holding potential (V_h) of −80 mV. In upper traces, currents in the control solution (◂–) and in the presence of 0·1 μM TTX (◃–) were superimposed. Lower traces were computed by subtracting the current in the presence of TTX from the current in the control solution. The cell shown in *Aa* had only the TTX-sensitive Na^+ channels (TTX-sensitive cell). The cell in *Ab* had only the TTX-insensitive Na^+ channels (TTX-insensitive cell). The cell in *Ac* had both types of Na^+ channels (partially TTX-sensitive cell). *B*, current–voltage relationships for TTX-sensitive and TTX-insensitive components of I_{Na} in the partially TTX-sensitive cell. A family of currents was evoked by a 30 ms step to various potentials from V_h of −80 mV in the control solution (◂–) and in the presence of 0·1 μM TTX (◃–). The current traces evoked by test potentials to −25, −10, +10, and +35 mV are illustrated. The TTX-sensitive components were isolated by subtraction as in *A*. The graph illustrates current–voltage curves. ○, I_{Na} in the control solution; ●, I_{Na} in the presence of TTX; □, TTX-sensitive component of I_{Na} obtained by subtraction. In this and subsequent figures, recordings from TTX-sensitive cells were performed in control solution and recordings form TTX-insensitive cells were performed in the presence of 1–2 μM TTX, unless otherwise stated: downward and upward deflections represent inward and outward currents, respectively.

In the third group of neurones, I_{Na} was partially blocked by TTX (partially TTX-sensitive cells, *Ac*). In the partially TTX-sensitive cells, the proportion of the TTX-sensitive component of I_{Na} to the TTX-insensitive component varied from cell to cell. As shown in the traces in Fig. 1*A* where current amplitudes were normalized to facilitate the comparison, the TTX-sensitive I_{Na} (*Aa*) had much faster activation and inactivation time courses than the TTX-insensitive I_{Na} (*Ab*). It has been reported that replacement of intracellular K^+ with Na^+ slows down I_{Na} kinetics (Chandler & Meves, 1970; Gillespie & Meves, 1981). Therefore, we compared I_{Na}s recorded in Cs^+-loaded or K^+-loaded pipette (10 cells, respectively). There was no detectable difference in the activation phase of I_{Na} between two groups.

In the partially TTX-sensitive cell, TTX-sensitive and TTX-insensitive components could easily by separated by TTX. As shown in Fig. 1*B*, the TTX-sensitive component (Control − TTX) was isolated by subtracting the current remaining in the presence of TTX (open arrow) from the total I_{Na} (filled arrow). The current–voltage curves in the partially TTX-sensitive cell (graph in Fig. 1*B*) show that the activation level was −60 mV for the TTX-sensitive component and −40 mV for the TTX-insensitive component. The maximal inward current was observed at −30 and 0 mV for the TTX-sensitive and TTX-insensitive components, respectively. The overlapping of the current–voltage curves for the total I_{Na} (open circles) and the TTX-sensitive component of I_{Na} (open squares) was due to large differences in the time course and amplitude of the TTX-sensitive and TTX-insensitive components (see Fig. 1*A*).

The current–voltage curve for I_{Na} in the TTX-sensitive cell was essentially identical to that for the TTX-sensitive component of I_{Na} in the partially TTX-sensitive cell (not illustrated). Similarly, the curve for I_{Na} in the TTX-insensitive cell was identical to that for the TTX-insensitive component of I_{Na} in the partially TTX-sensitive cell (not shown). Close measurement of the activation threshold in 1 mV step increases showed that the activation threshold was $-57{\cdot}6 \pm 0{\cdot}7$ mV for the TTX-sensitive I_{Na} and $-35{\cdot}9 \pm 1{\cdot}0$ mV for TTX-insensitive I_{Na}, and that the maximum current occurred at $-30{\cdot}2 \pm 0{\cdot}8$ mV for TTX-insensitive I_{Na} and $-0{\cdot}5 \pm 0{\cdot}7$ mV for TTX-insensitive I_{Na} ($n = 10$ in all cases).

In experiments reported here, TTX-sensitive and TTX-insensitive cells were mainly used. Although the TTX-insensitive cells which we have used were devoid of any detectable TTX-sensitive component, TTX in concentrations over 0·1 μM, which caused total suppression of the TTX-sensitive I_{Na} (see below), was included in the external solution in recordings of the TTX-insensitive I_{Na}, unless otherwise stated.

Sodium dependence of TTX-insensitive I_{Na}

Figure 2 confirms that the TTX-insensitive inward current observed above is indeed produced by an influx of Na^+ ions. A family of inward currents in the control solution (*Aa*) was decreased by 0·1 μM TTX (*Ab*). When the Na^+ in the medium was totally removed in the presence of TTX, the current traces became much smaller and the polarity of the current became outward (*Ac*). As shown in the graph of Fig. 2*A*, the reversal potential shifted in the hyperpolarizing direction when the external Na^+ concentration was reduced, whereas the activation threshold remained constant. Thus, it is concluded that the TTX-insensitive inward current is in fact generated by an influx of Na^+ ions.

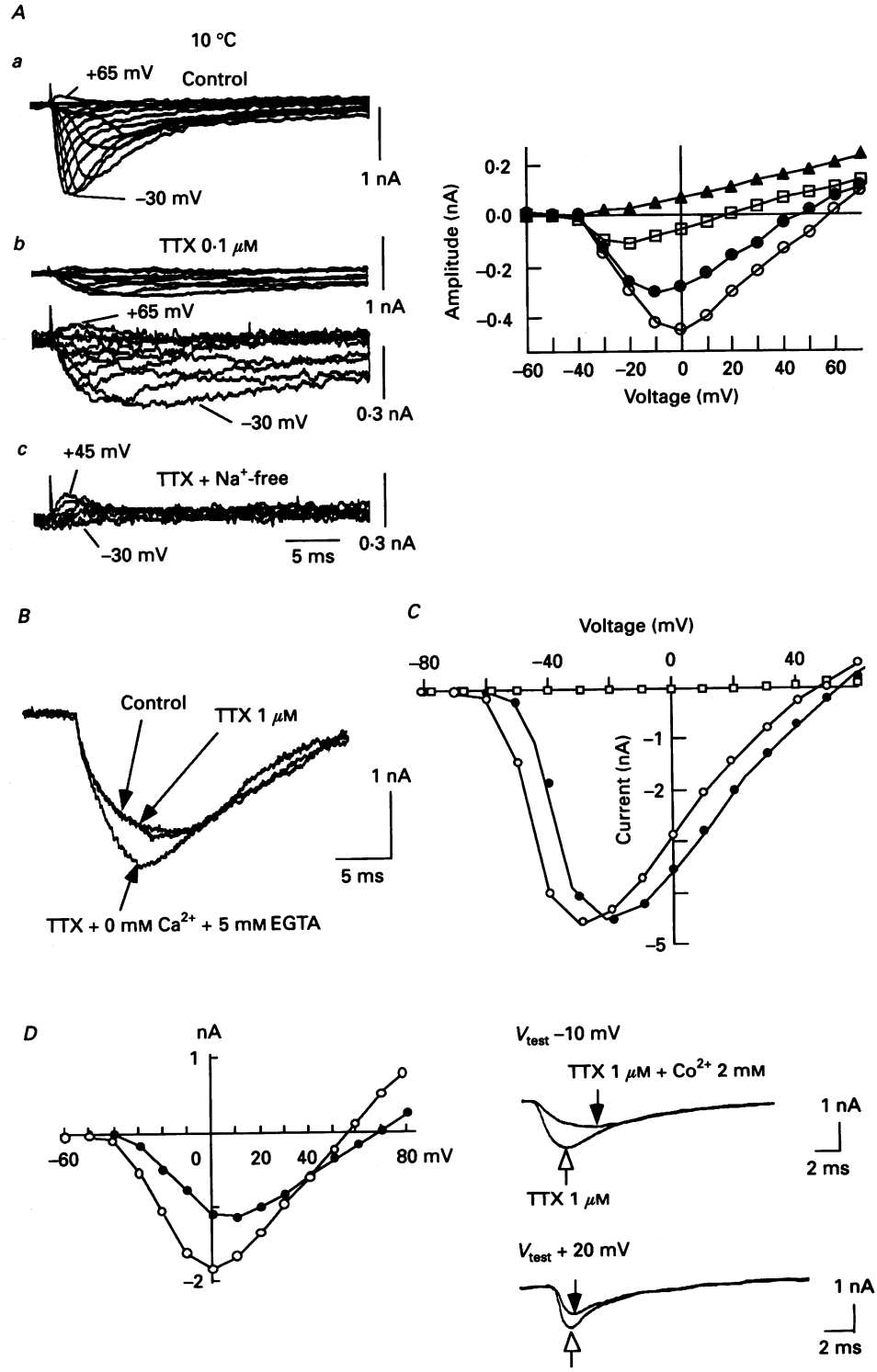

Fig. 2. For legend see facing page.

Since in our experiments, fluorine was used as the internal anion, which completely suppresses Ca^{2+} currents in rat DRG, the possibility of an involvement of Ca^{2+} currents can be excluded. This was further confirmed in the experiment shown in Fig. 2*B*. I_{Na} which was insensitive to TTX (0·1 μM) was not abolished in a solution in which 5 mM EGTA was added in addition to TTX and Ca^{2+} was totally removed. The peak amplitude was rather increased and the activation phase was accelerated possibly through a change in surface potential.

The slow TTX-insensitive Na^+ channel is reminiscent of the Ca^{2+} channel in its insensitiveness to TTX and relatively slow time course of activation and inactivation. Therefore, we studied the sensitivity of I_{Na} to divalent cations. A concentration of Cd^{2+} of 50 μM, which produces a total suppression of Ca^{2+} currents in rat DRG neurones (Tatebayashi & Ogata, 1992), had no effect on either the TTX-sensitive or TTX-insensitive I_{Na}. TTX-sensitive I_{Na} was not inhibited by a high concentration (2 mM) of Co^{2+}, although the voltage axis of the activation was shifted in the depolarizing direction by about 10 mV (Fig. 2*C*), due to surface charge effects of Co^{2+} (Frankenhaeuser & Hodgkin, 1957). On the contrary, TTX-insensitive I_{Na} was moderately inhibited by Co^{2+}. The inhibition was not due to shift in the voltage axis, because it was observed at the test pulses to both −10 mV and +20 mV (Fig. 2*D*). As indicated by the delay of the time to peak (compare open and filled arrows), there is a shift of voltage axis. Thus, true inhibition was calculated by comparing the peak amplitudes of the current–voltage curves. TTX-insensitive I_{Na} was decreased to 59·8 ± 7·0% ($n = 5$) of the control.

Concentration–response relationships for TTX

The TTX-insensitive I_{Na} was not affected by an extremely high concentration of TTX (100 μM). On the contrary, TTX in nanomolar concentrations effectively blocked the TTX-sensitive Na^+ current (Fig. 3*A*). The concentration of TTX required for a 50% block of I_{Na} (dissociation constant, K_d) obtained from the concentration–response curve based on ten measurements was 3·3 nM (Fig. 3*B*). This value is in close agreement with K_d values reported in other preparations (e.g. 3–5 nM

Fig. 2. *A*, dependence of TTX-insensitive I_{Na} on external Na^+. A family of currents was evoked by a 30 ms step to various potentials from V_h of −80 mV in control solution (*Aa*), in the presence of 0·1 μM TTX (*Ab*), and in the presence of TTX solution containing no external Na^+ (*Ac*). Two sets of traces in *Ab* were the same traces with different magnifications. The graph illustrates current–voltage curves obtained in external media with different Na^+ concentrations. Peak amplitude of I_{Na} was plotted against the test potential, $[Na^+]_o$ ○, 100 mM (normal); ●, 50 mM, □, 25 mM; △, 0 mM. Current traces in *A* were made at a medium temperature of 10 °C, since, under low temperatures, the recording condition was markedly improved and a long period of stable recording was possible. *B*, I_{Na} was evoked by a step depolarization to −10 mV from V_h of −80 mV in the control, in the presence of TTX, or in the medium which were Ca^{2+}-free and contained 1 μM TTX and 5 mM EGTA. Although the cell perfused with solution containing EGTA immediately deteriorated, there was enough time to record I_{Na}. *C*, effects of Co^{2+} on the TTX-sensitive I_{Na}. Current–voltage curves were measured in control (○), in the presence of 2 mM Co^{2+} (●), and in the presence of 1 μM TTX (□). *D*, effects of Co^{2+} on the TTX-insensitive I_{Na}. Current–voltage curves were measured in the presence of 1 μM TTX (○), and in the presence of 1 μM TTX plus 2 mM Co^{2+} (●). Current traces evoked by test pulses to −10 mV and +20 mV were illustrated. Arrows (◁– and ◀–) indicate the peak amplitudes. *A*, partially TTX-sensitive cell: *B* and *D*, TTX-insensitive cells: *C*, TTX-sensitive cell.

in squid giant axons (Cuervo & Adelman, 1970) and 3·18 nM in myelinated nerve fibers (Colquhoun & Ritchie, 1972).

The concentration–response relationship was best fitted by the curve calculated on the basis of 2 to 1 stoichiometry. This stoichiometry is in remarkable contrast with

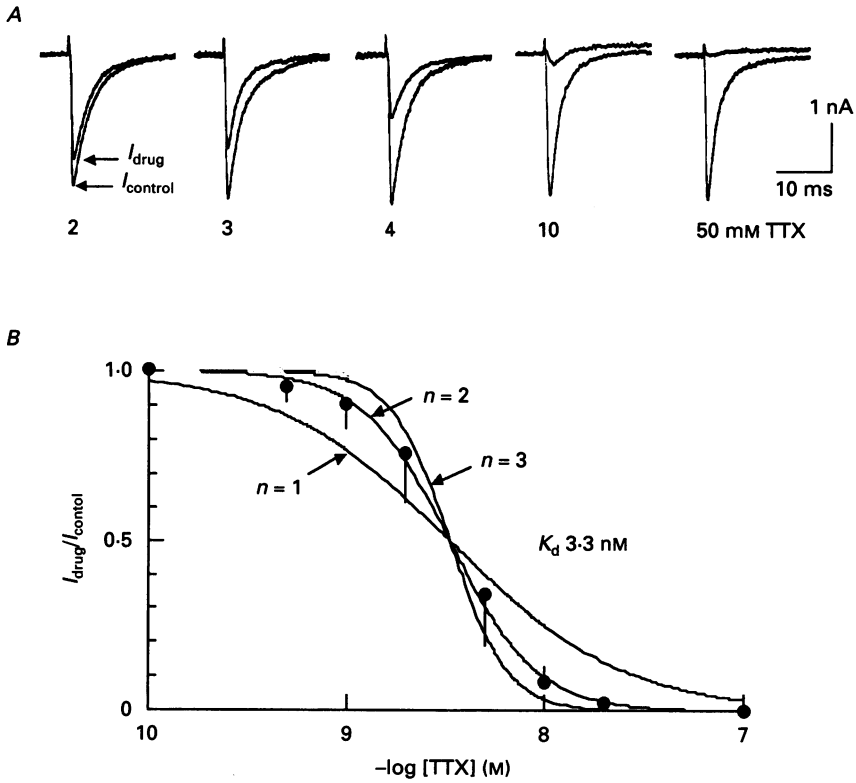

Fig. 3. Concentration–response relationships for the inhibition of TTX-sensitive I_{Na} by TTX. *A*, currents were evoked in a TTX-sensitive cell by a step depolarization to −10 mV from V_h of −80 mV. Each pair of superimposed current traces was recorded in the presence or absence of TTX. *B*, concentration–response curves measured in TTX-sensitive cells. The data points were fitted by sigmoidal curves calculated from the following equation based on n to 1 stoichiometry for interaction of TTX molecules with binding sites with an apparent dissociation constant (K_d) of 3·3 nM.

$$I_{Na} = 1/\{1+([TTX]/K_d)^n\},$$

where [TTX] represents the TTX concentration. The vertical lines represent S.E.M.

the 1 to 1 stoichiometry reported for other preparations, e.g. rabbit Purkinje fibres (Cohen, Bean, Colatsky & Tsien, 1981) or neuroblastoma cells (Quandt, Yeh & Narahashi, 1985). This may be due to a species difference, since in our experiments, the 2 to 1 stoichiometry was reproducible in all ten cells examined. Furthermore, 50 nM TTX consistently produced total suppression of the TTX-insensitive I_{Na}, while 1 nM TTX produced only a slight inhibition in almost all the cells examined. Such a relationship between the concentration and response cannot be explained by 1 to 1 stoichiometry (see the curve in Fig. 3*B* based on 1 to 1 stoichiometry).

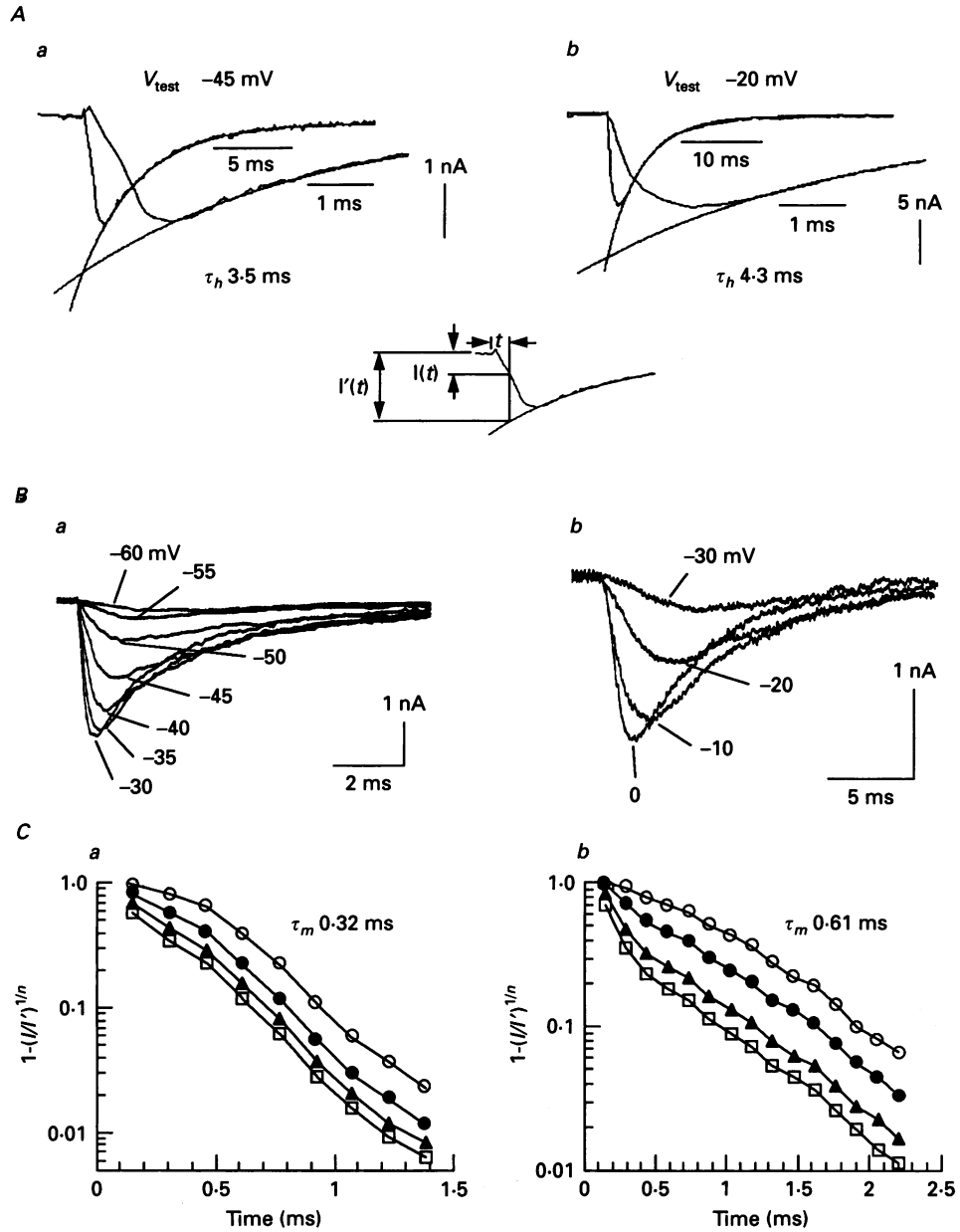

Fig. 4. Activation parameters of the two types of I_{Na}. The channel activation was assessed by eqn (3) described in the text. Inset schematizes the parameters in eqn (3). $I(t)$ represents the recorded current amplitude at time t. $I'(t)$ represents the current amplitude estimated by the extrapolation of the decay phase fitted by an exponential function. *A* illustrates a single exponential fit of the decay phase of I_{Na} evoked by a test pulse to −45 mV in the TTX-sensitive cell (*Aa*) or evoked by a test pulse to −20 mV in the TTX-insensitive cell (*Ab*). The same current recordings are illustrated with different time scales. A family of currents in *B* was evoked by step depolarizations to various potentials within a range of negative slope region of the current–voltage curve, from V_h of −80 mV. *C*, the value, $1-[I(t)/I'(t)]^{1/n}$, was plotted against time t on a semilogarithmic scale. The

Activation kinetics

According to the Hodgkin–Huxley formulation (Hodgkin & Huxley, 1952), the time course of I_{Na} can be described as:

$$I(t) = A\, m_t^n\, h_t, \tag{1}$$

where A is a constant, m_t and h_t are the dimensionless kinetic parameters at time t for activation and inactivation, respectively, which varies between 0 and 1, and n is an integer. The parameters, m_t and h_t, change exponentially with time following a step change of the membrane potential:

$$m_t = (m_0 - m_\infty)\exp(-t/\tau_m) + m_\infty,$$

$$h_t = (h_0 - h_\infty)\exp(-t/\tau_h) + h_\infty,$$

where m_0 and h_0 refer to the values at $t = 0$ (at the beginning of the pulse), m_∞ and h_∞ are their steady-state during the pulse, and τ_m and τ_h are the time constants of m and h, respectively. For the decaying phase of the I_{Na}, i.e. for $t \gg \tau_m$, m can be approximated by m_∞. If the membrane is stepped from a potential negative to the channel activation level, m_0 is regarded as zero. Thus, the decay phase of I_{Na} can be described as:

$$I'(t) = A\, m_\infty^n\, h_t. \tag{2}$$

$I'(t)$ values at the times $0 < t < \tau_m$, can be obtained by extrapolation of the current decay (see inset of Fig. 4). Eqns (1) and (2) yield a relation in which the voltage-dependent constant, m_∞, and the voltage- and time-dependent parameter, h_t, are removed:

$$I(t)/I'(t) = [1 - \exp(-t/\tau_m)]^n$$

$$\text{i.e. } \exp(-t/\tau_m) = 1 - [I(t)/I'(t)]^{1/n}. \tag{3}$$

Thus, the plot of the value, $1-[I(t)/I'(t)]^{1/n}$, against t on a semilogarithmic scale should fall on a straight line if an appropriate integer is given to n. As shown in Fig. 4*A*, the decay of I_{Na} followed a single exponential time course in both TTX-sensitive (*Aa*) and TTX-insensitive (*Ab*) I_{Na}. Therefore, the values for $I'(t)$ were calculated from the single exponential curve which gave a best fit to the recorded decay phase of I_{Na}. For accurate measurements of $I(t)$ and $I'(t)$, reliable voltage and space clamp controls are indispensable. As shown in Fig. 4*B*, there was no 'threshold phenomenon' and currents increased gradually in the negative slope region of the current–voltage curve in both TTX-sensitive (*Ba*) and TTX-insensitive (*Bb*) I_{Na}, indicating excellent voltage-clamp control (Jack, Noble & Tsien, 1983). As shown in Fig. 4*Ca*, the plot for the TTX-sensitive I_{Na} fell on a straight line when n was 3. Thus, the activation process is best described by m^3 kinetics. In contrast to the TTX-sensitive I_{Na}, the activation process for the TTX-insensitive I_{Na} was best described by m^1 kinetics (Fig. 4*Cb*).

---

activation time constant, τ_m, was calculated from the slope of the plot. *Ca*, TTX-sensitive cell; ○, $n = 1$; ●, $n = 2$; ▲, $n = 3$; □, $n = 4$; *Cb*, TTX-insensitive cell; (○, $n = 0{\cdot}5$; ●, $n = 1$; ▲, $n = 2$; □, $n = 3$.

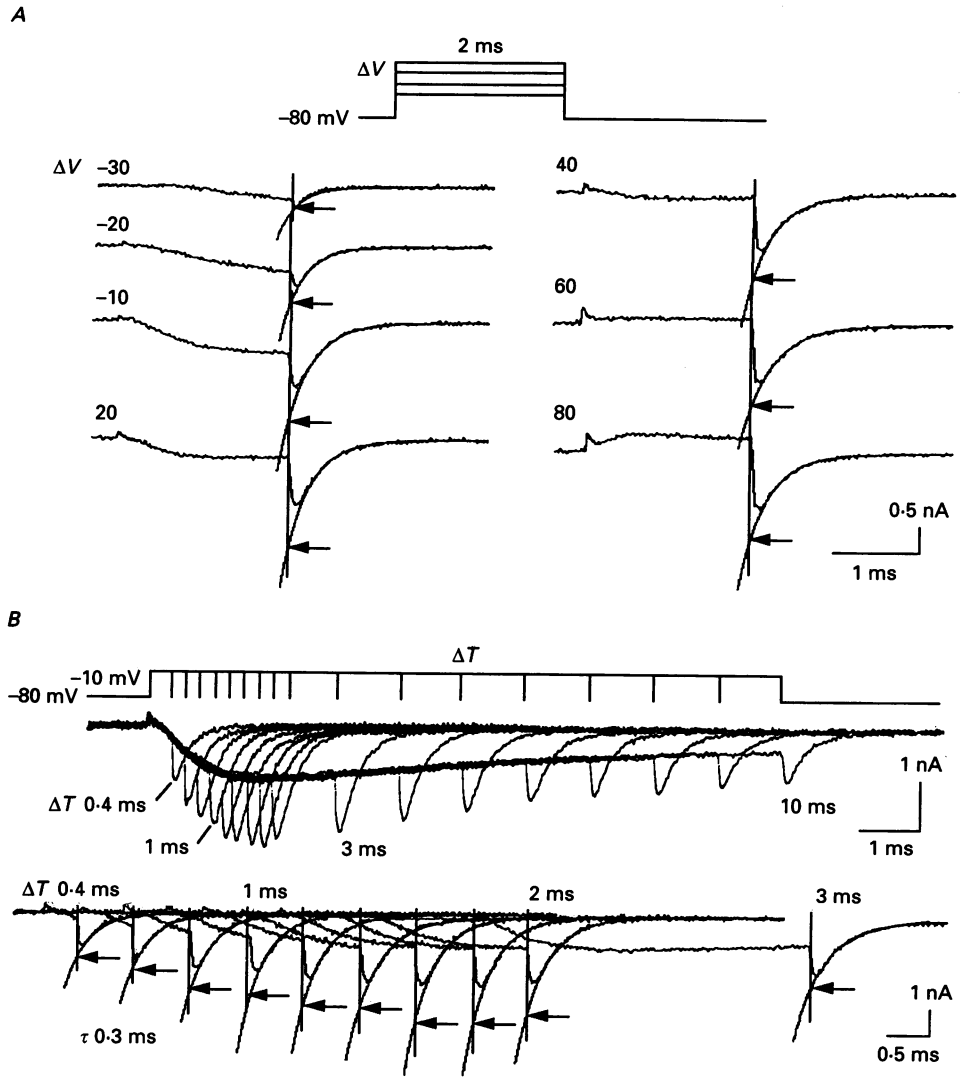

Fig. 5. Time course of deactivation of the TTX-insensitive I_{Na}. *A*, tail currents associated with step repolarization to V_h (−80 mV) from depolarizing pulses to various potential levels (ΔV, in mV). The duration of the depolarizing pulses was fixed at 2 ms. *B*, tail currents associated with step repolarization to V_h (−80 mV) from depolarizing pulses of various durations (ΔT). The potential level of the depolarizing pulses was fixed at −10 mV. Continuous lines represent single exponential curves fitted to the tail current (time constant, 0·3 ms in all the traces). The initial amplitude of the tail current represented by ←, determined by extrapolating the falling phase to the time of repolarization. *A* and *B* were recorded from the same TTX-insensitive cell.

Steady-state activation

The instantaneous current upon repolarization (tail current) was measured to study the voltage dependence of activation at the steady-state (m_∞). Figure 5*A* shows the tail currents observed in the TTX-insensitive I_{Na} upon clamp-back to a

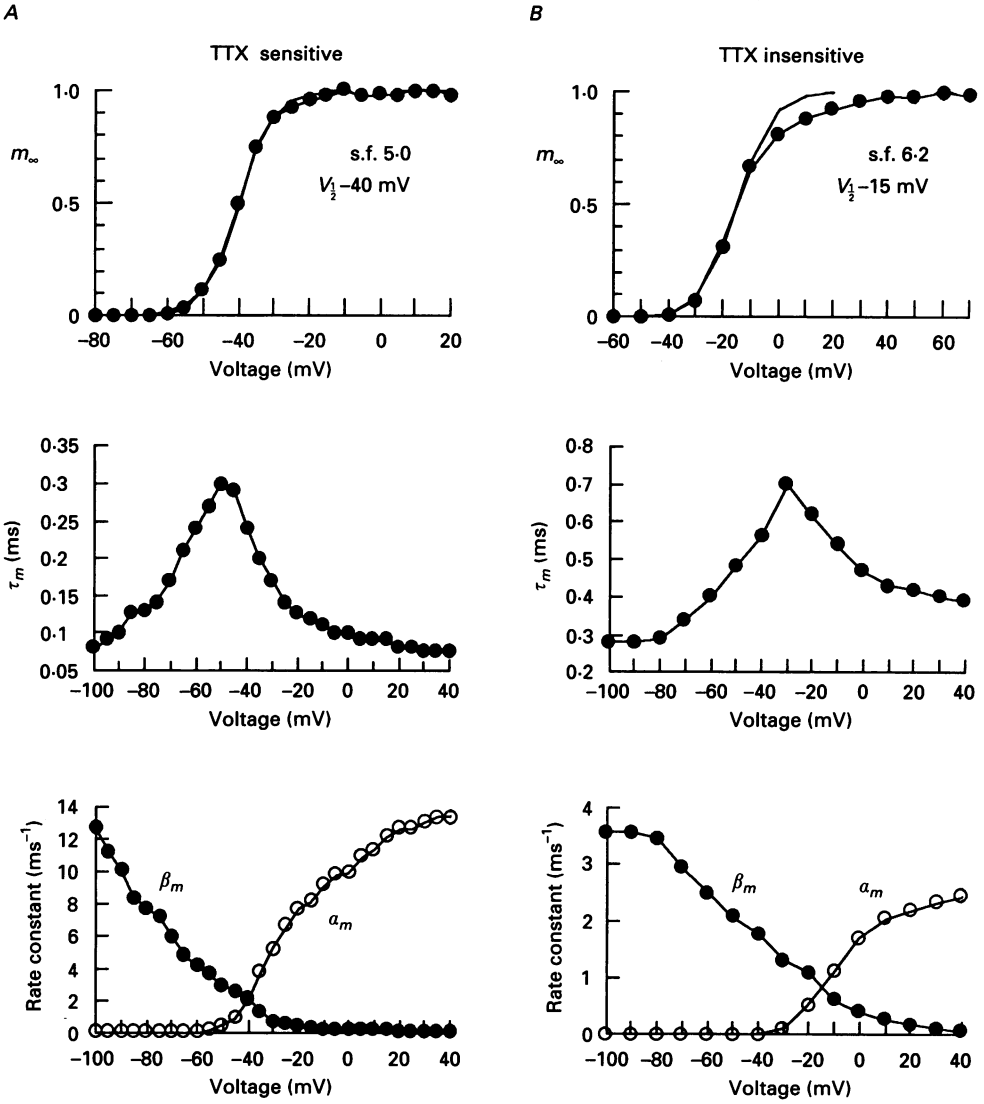

Fig. 6. Steady-state activation (m_∞) curves, time constants of activation (τ_m) and rate constants for TTX-sensitive (*A*) and TTX-insensitive (*B*) I_{Na}. The m_∞ value was calculated as the cubic root (because parameter m for the TTX-sensitive I_{Na} was 3, see Fig. 4*A*) of the maximal amplitude of the tail current obtained at each test potential (see Fig. 5*B*) for the TTX-sensitive I_{Na}. The m_∞ value for the TTX-insensitive I_{Na} was the maximal amplitude of the tail current (because parameter m for the TTX-insensitive I_{Na} was 1, see Fig. 4*B*). The m_∞ values were normalized and plotted against the potential level. The τ_m values at potentials positive to −45 mV (TTX-sensitive I_{Na}) and −30 mV (TTX-insensitive I_{Na}) were obtained according to the method described in Fig. 4. The τ_m values at potentials negative to −50 mV (TTX-sensitive I_{Na}) and −40 mV (TTX-insensitive I_{Na}) were obtained from the decay time course of the tail current. Forward (α_m) and backward (β_m) rate constants were calculated using the following equations:

$$\alpha_m = m_\infty/\tau_m; \quad \beta_m = (1-m_\infty)/\tau_m.$$

fixed potential (−80 mV) from various voltages (ΔV). The deactivation time course of the tail current was expressed by a single exponential function in all the traces with different ΔV. The initial portion of the tail current became rounded after the P-P/4 procedure due to limited sampling interval (10 μs) of analog-to-digital conversion. However, this did not affect the exponential fitting of the decaying phase of the tail current, since the duration of this was much shorter than the decay time constant of the tail current.

The tail current with maximal amplitude at a given potential level was obtained at a different time after the onset of step depolarization depending on the level of the step depolarization. Therefore, the maximal amplitude of the tail current for a given potential level was determined by measuring the time dependence of the tail current amplitude by changing the duration of the step depolarization (ΔT) with 0·2 ms increments (Fig. 5*B*).

At the onset of repolarization, m_t is considered to be the maximal value of m at respective levels, i.e. m_∞. If we assume that the value of h_t at the onset of repolarization is nearly 1, then, from eqn (1), the m_∞ value can be expressed as: $m_\infty = A[I_{(t)}]^{1/n}$, where A is a constant and n is 3 for TTX-sensitive I_{Na} and 1 for TTX-insensitive I_{Na} (see Fig. 4). The m_∞ curves for TTX-sensitive (*A*) and TTX-insensitive (*B*) I_{Na} were illustrated in the upper graphs of Fig. 6. The slope factor for a change by a factor of e in the m_∞ and the mid-point potential ($V_{\frac{1}{2}}$) were, respectively 5·2±0·6 mV and −41·3±2·1 mV ($n = 4$) for the TTX-sensitive I_{Na} and 6·0±0·5 mV and −16·1±2·3 mV ($n = 4$) for the TTX-insensitive I_{Na}.

Time course of activation

The activation time constant, τ_m, was measured by the method shown in Fig. 4. The value of τ_m for TTX-sensitive I_{Na} showed an exponential decrease in the range between −45 and −20 mV, and remained relatively constant at potentials positive to −20 mV (Fig. 6*A*). The τ_m for the TTX-insensitive I_{Na} (Fig. 6*B*) had less prominent voltage dependence compared with the voltage dependence of τ_m for the TTX-sensitive I_{Na}, and the steady-state value at the depolarized membrane potentials were about four times longer than that for the TTX-sensitive I_{Na}.

To determine the forward (or activation) and the backward (or deactivation) rate constants, a first-order kinetic model (Hodgkin & Huxley, 1952) was applied as a first approximation of the activation process of Na^+ channels. The following relations were used to calculate these rate constants:

$$\alpha_m = m_\infty/\tau_m; \quad \beta_m = (1-m_\infty)/\tau_m,$$

where α_m and β_m are the forward and backward rate constants, respectively. The forward rate constant for the TTX-sensitive I_{Na} was 4–5 times faster than that of the TTX-insensitive I_{Na} when values were compared within a comparable voltage

---

The smooth curves in the m_∞ curves were drawn according to the equation: $m_\infty = 1/(1+\exp[V_{\frac{1}{2}}-V_{test})/\kappa])$, where V_{test} is the potential level of the test pulse, $V_{\frac{1}{2}}$ is the V_{test} where m_∞ is one-half maximal, and κ is the slope factor. *A*, TTX-sensitive cell: *B*, TTX-insensitive cell.

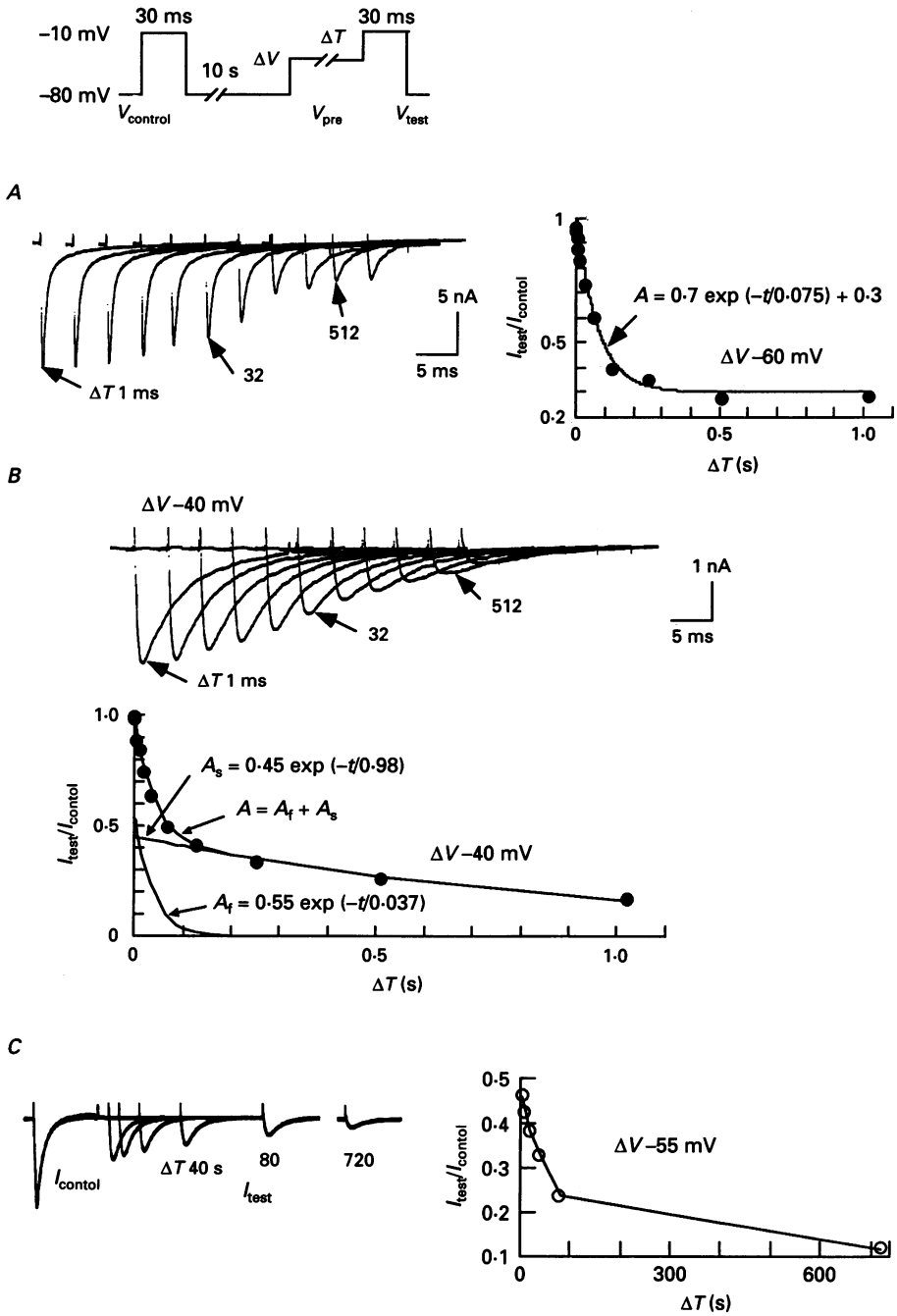

Fig. 7. Time-dependent inactivation of I_{Na}. Inset illustrates experimental protocol. Two identical step depolarizations to -10 mV for 30 ms were applied 10 s prior ($V_{control}$) and immediately subsequent (V_{test}) to the conditioning prepulse (V_{pre}). The potential level (ΔV) and the duration (ΔT ms) of V_{pre} was changed to various values. *A*, current traces observed in the TTX-sensitive cell in response to V_{test} are shown overlapped at regular intervals.

range (-10 to $+10$ mV), whereas the backward rate constant was much the same as that for the TTX-insensitive I_{Na} (bottom graphs in Fig. 6). This indicates that activation of the TTX-sensitive Na^+ channels occurs much faster than that of the TTX-insensitive Na^+ channels, whereas the velocity of channel deactivation is similar.

Onset of inactivation

Figure 7 illustrates the time dependence of the inactivation process of TTX-sensitive and TTX-insensitive I_{Na}. The TTX-sensitive I_{Na} was rapidly inactivated by a prepulse applied immediately prior to V_{test} and its time course was described by a single exponential (Fig. 7*A*). On the other hand, the time course of inactivation of TTX-insensitive I_{Na} was described by at least two exponentials (Fig. 7*B*). A striking feature of the inactivation process of the TTX-insensitive I_{Na} is that it proceeds extremely slowly during a maintained depolarizations. As shown in Fig. 7*C*, even at 720 ms, the inactivation does not reach a plateau. 'True' steady-state current could be obtained after 180 s (not illustrated). This kind of slow inactivation has been reported in Na^+ channels of myelinated nerve (Fox, 1976) or of cardiac Purkinje fibres (Carmeliet, 1987*b*) and in Ca^{2+} channels of ventricular myocytes (Schouten & Morad, 1989). We further describe this process in DRG neurones elsewhere (Ogata & Tatebayashi, 1992*b*).

Steady-state inactivation

Figure 8 shows the potential dependence of Na^+ channel availability for the TTX-sensitive I_{Na} obtained with a conditioning depolarization (prepulse) of 0·5 s. In order to minimize the error arising from possible fluctuations of I_{Na}, the control I_{Na} was measured 10 s prior to each V_{test}. This interval was sufficient to allow recovery from inactivation following $V_{control}$. Experiments in which the amplitude of $V_{control}$ changed more than 5% were discarded. Figure 8*A* illustrates current traces evoked by $V_{control}$ ($I_{control}$) and V_{test} (I_{test}). A plot of the ratio, $I_{test}/I_{control}$ against V_{pre} gives a measure of the voltage dependence of inactivation at time 0·5 s ($h_{0.5}$) (Fig. 8*B*) where V_{pre} is conditioning prepulse. The curve obtained with 30 s prepulses (filled circles) was much the same as the curve obtained with 0·5 s prepulses (open circles). The $h_{0.5}$ curve had a slope factor of 5·1 mV (5·2 ± 0·2 mV, $n = 4$) and a mid-point voltage ($V_{\frac{1}{2}}$) of -64 mV ($-64·3 \pm 0·8$ mV, $n = 4$).

The $h_{0.5}$ curve for the TTX-insensitive I_{Na} was shifted about 25 mV in the positive

---

The peak current amplitude measured during V_{test} was divided by the peak amplitude measured during a matching $V_{control}$ and plotted as a function of ΔT. The smooth curve was drawn according to the equation:

$$I_{test}/I_{control} = 0·7 \exp(-\Delta t/0·075) + 0·3.$$

B, the same as *A*, but here I_{Na} was recorded from the TTX-insensitive cell, (ΔT ms). The plot was best described by the sum of the following two exponentials:

$$A_f = 0·55 \exp(-t/0·037), \quad A_s = 0·45 \exp(-t/0·98).$$

C, the same as in *B* but the plot was made with much longer ΔT, (ΔT s). Currents evoked by $V_{control}$ ($I_{control}$) are shown superimposed and currents evoked by V_{test} (I_{test}) are shown at increasing intervals. *B* and *C* were recorded from the same TTX-insensitive cell.

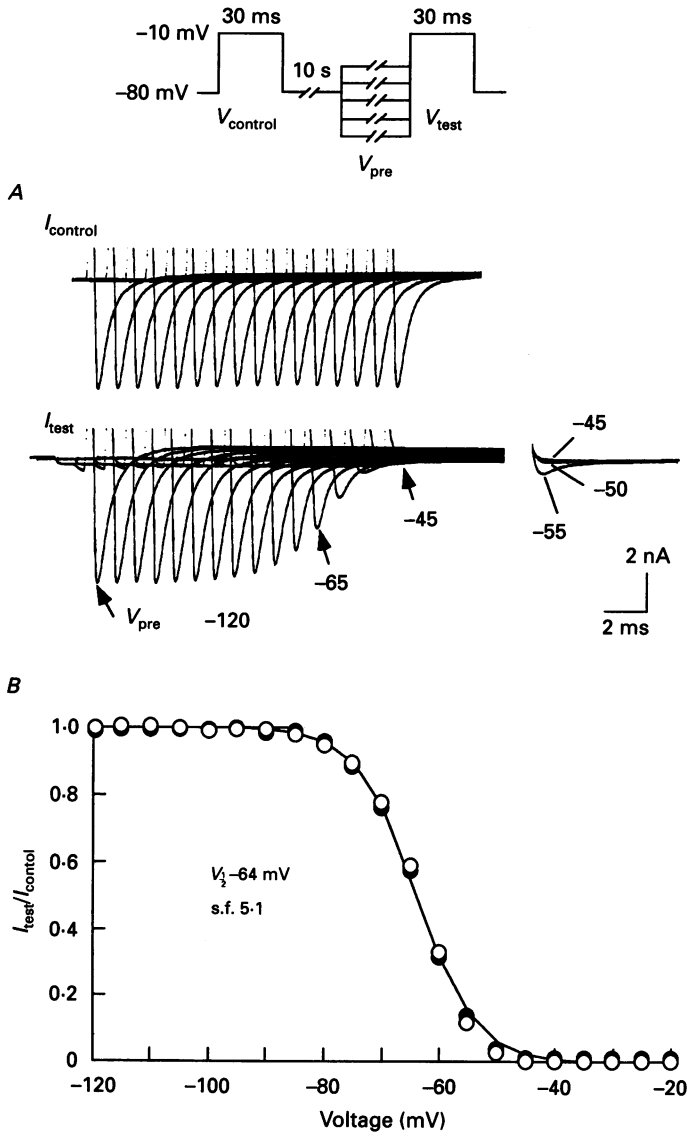

Fig. 8. Steady-state inactivation curves obtained in a TTX-sensitive cell. Inset illustrates experimental protocol. Two identical step depolarizations to −10 mV for 30 ms were applied 10 s prior ($V_{control}$) and immediately subsequent (V_{test}) to the conditioning prepulse (V_{pre}) from V_h of −80 mV. The potential level of V_{pre} was changed from −120 mV to −20 mV in 5 mV steps. *A*, currents evoked by $V_{control}$ ($I_{control}$) and currents evoked by V_{test} (I_{test}) are shown overlapped at regular intervals. I_{test} in response to step depolarizations to −55, −50 and −45 mV are also shown superimposed. *B*, the peak amplitude of I_{test} was divided by the peak amplitude of matching $I_{control}$ and plotted as a function of V_{pre}. The smooth curves were drawn according to the following equation:

$$I_{test}/I_{control} = 1/(1+\exp[(V_{pre}-V_{\frac{1}{2}})/\kappa]),$$

where $V_{\frac{1}{2}}$ is the V_{pre} where I_{Na} is one-half maximal, and κ is the slope factor. Duration of V_{pre} was 0·5 s (○) or 30 s (●).

direction as compared with the curve for the TTX-sensitive I_{Na} (Fig. 9*B*). In contrast to $h_{0.5}$ for the TTX-sensitive I_{Na}, $h_{0.5}$ values became progressively smaller when the prepulse level was hyperpolarized (see I_{test} of Fig. 9*A*). The $h_{0.5}$ curve for the TTX-insensitive I_{Na} had a slope factor of 4·2 mV (4·6±0·3 mV, $n = 4$) and a $V_{\frac{1}{2}}$ of −39 mV (−40·1±0·8 mV, $n = 4$).

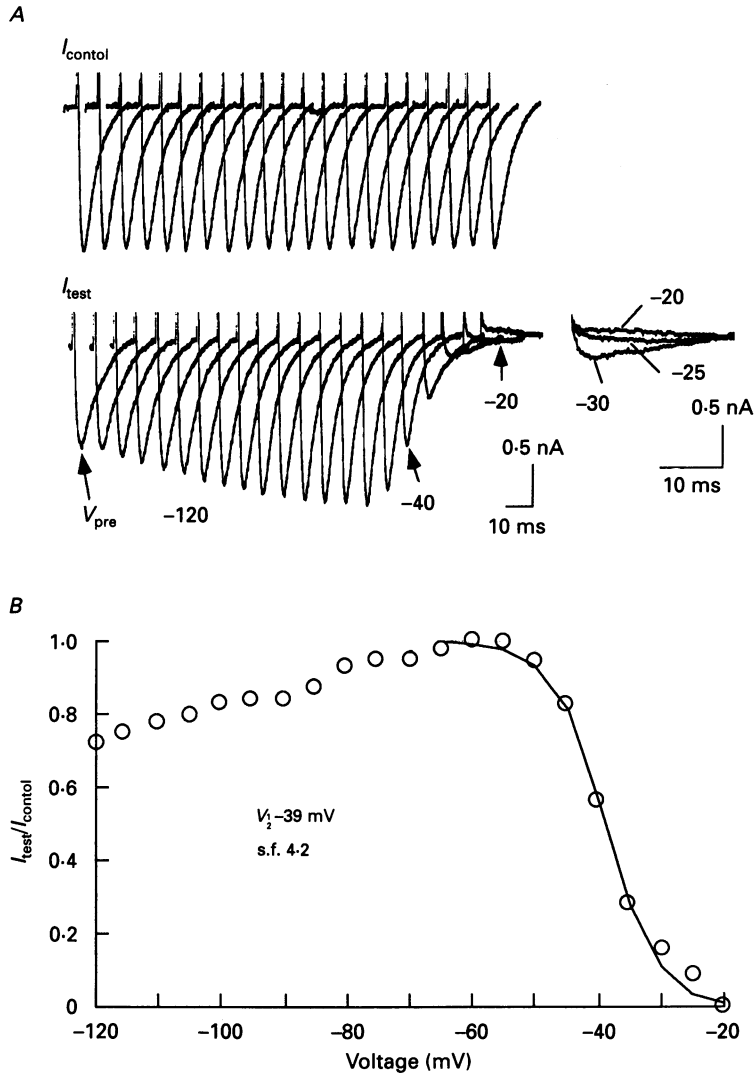

Fig. 9. Voltage dependence of the Na^+ channel availability in a TTX-insensitive cell. Experimental protocol is the same as in Fig. 8. The duration of V_{pre} was 0·5 s and values are quoted in mV.

The $h_{0.5}$ curve for I_{Na} of a partially TTX-sensitive cell is shown in Fig. 10. The overlapped or superimposed traces of successive I_{test} in response to V_{pre} from −140 to −35 mV in 5 mV steps (Fig. 10*A*) showed an apparent inflexion, indicating the

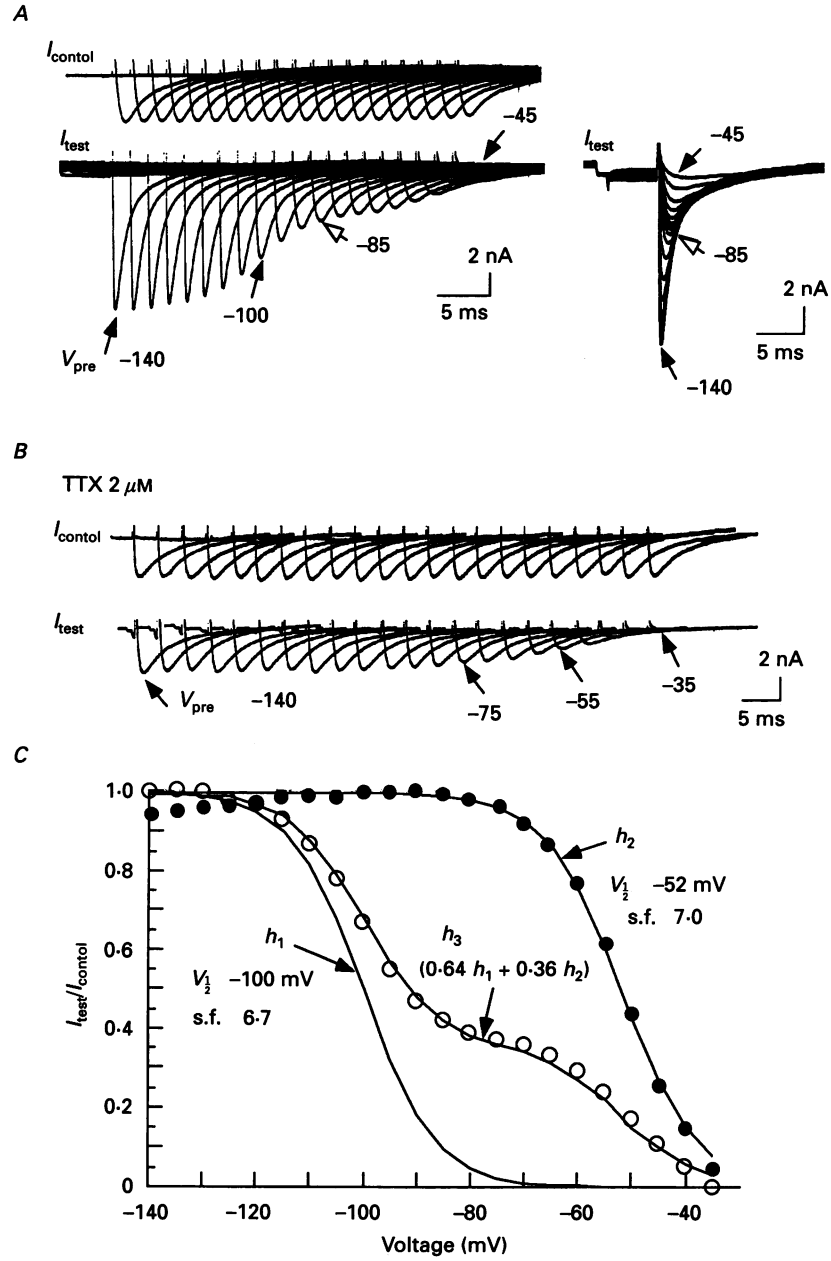

Fig. 10. Modulation of Na^+ channel availability by TTX in a partially TTX-sensitive cell. Experimental protocol was the same as in Fig. 8. The duration of V_{pre} was 0·5 s. In *A*, I_{test} are also shown superimposed to facilitate the illustration of the inflection on the envelope of the successive peak I_{Na} (⇦ labelled −85 mV). *A* was recorded in the control solution, all values are in mV. *B* was recorded in the presence of 2 μM TTX, quoted values in mV. *C*, inactivation curves for the total I_{Na} measured in control solution (○) and for the TTX-insensitive component of I_{Na} measured in the presence of 2 μM TTX (●). h_1 and h_2 are the theoretical curves calculated with $V_{\frac{1}{2}}$ of −100 mV and −52 mV and slope factor (s.f.) of 6·7 and 7·0, respectively. h_3 was calculated by (0·64 h_1 + 0·36 h_2).

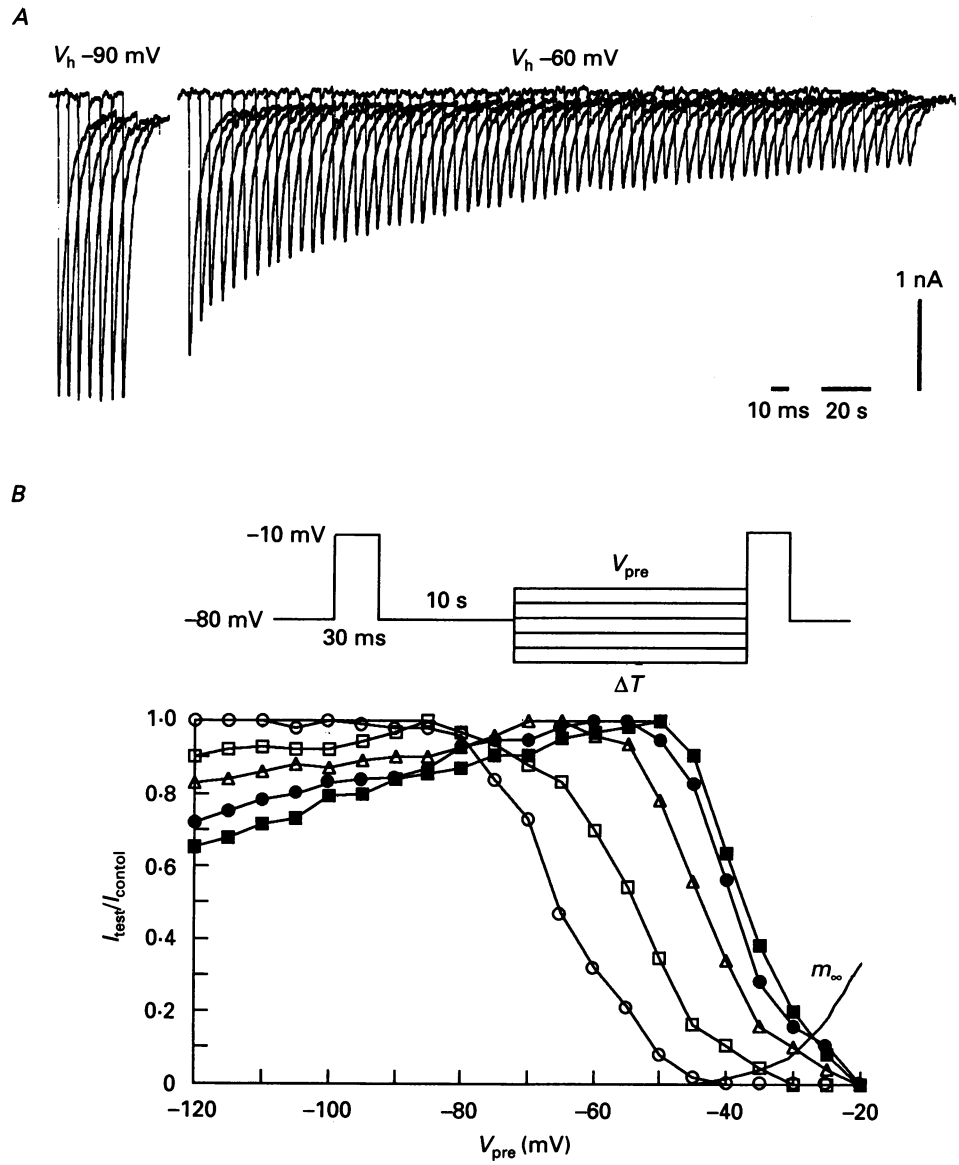

Fig. 11. Time dependence of Na^+ channel availability in TTX-insensitive cells. *A*, slow inactivation of TTX-insensitive I_{Na}. I_{Na} was evoked by a voltage step to −10 mV from V_h of −90 mV (left traces) and subsequently from V_h of −60 mV (right traces). Between two groups of differing V_h, 10 s was interposed. *B*, experimental protocol is the same as in Fig. 8, but here the prepulse duration (ΔT) was changed from 50 ms to 5 min. ΔT: ■, 50 ms; ●, 500 ms; △, 1 s; □, 30 s and ○, 5 min. All measurements were made using the same cell. The m_∞ curve for the TTX-insensitive I_{Na} (Fig. 6*B*) is also shown.

existence of a voltage range in which inactivation is slowed. The h_∞ curve measured in the control solution (open circles in Fig. 10*C*) had an inflexion point at about −90 to −80 mV and apparently could not be described by the Bolzmann equation. The

$h_{0.5}$ curve was best fitted by a sum of the two Boltzmann distributions (h_3) in Fig. 10*C*). The two Boltzmann curves (h_1 and h_2 in Fig. 10*C*) had a $V_{\frac{1}{2}}$ of $-102{\cdot}2 \pm 2{\cdot}1$ mV and $-50{\cdot}5 \pm 1{\cdot}7$ mV ($n = 5$), respectively. In the presence of TTX, the peak amplitude of I_{Na} changed monophasically (Fig. 10*B*) and the h_∞ curve was fitted by a single Boltzmann equation with a $V_{\frac{1}{2}}$ of $-48{\cdot}2 \pm 1{\cdot}4$ mV ($n = 5$). Interestingly, $V_{\frac{1}{2}}$ for the h_∞curve of the TTX-sensitive component deviated markedly (about 35 mV) in the negative direction. This was reproducible in all five cells examined. This was not due to F^- which causes a time-dependent shift of the h_∞ curve in cardiac myocytes (Follmer, Ten Eick & Yeh, 1987; Ogata *et al.* 1989), since the shift was also observed when glutamate ions were used as the internal anion.

As there is a slow process of inactivation in the TTX-sensitive I_{Na} (see Fig. 7*C*), the inactivation curve for the TTX-insensitive I_{Na} showed change as a function of the prepulse duration. This was examined in Fig. 11. As shown in Fig. 11*A*, after a step to a positive V_h, the peak Na^+ current reaches its new steady-state level within about 4 min, indicating the existence of a markedly slow inactivation process in the TTX-insensitive I_{Na}. Thus, the voltage dependence of Na^+ channel availability was affected by the duration of the prepulse (Fig. 11*B*). The 'quasi' steady-state inactivation was obtained at a prepulse duration of 5 min.

Time course of inactivation

The inactivation time constant, τ_h, was measured directly from the decay phase of TTX-sensitive I_{Na} (Fig. 12*A*) or of TTX-insensitive I_{Na} (Fig. 12*B*) for suprathreshold potentials. The decay phase of I_{Na} evoked by step depolarizations to various potential levels could be approximated by a single exponential function when satisfactory voltage-clamp conditions were attained. This is in remarkable contrast to reports describing a two exponential decay of I_{Na} (e.g. Chiu, 1977; Patlak & Ortiz, 1985; Follmer *et al.* 1987; Ogata & Tatebayashi, 1990). τ_h values for the TTX-sensitive I_{Na} at subthreshold potentials were approximated by the fast component of the double exponential recovery process measured by a conventional double-pulse protocol (see Fig. 13). This approximation was based on the result that the amplitude of the fast component was more than nine times larger than that of the slow component. τ_h values for the TTX-insensitive I_{Na} at subthreshold potentials were not determined, since the definite recovery time constant for the TTX-insensitive I_{Na} could not be determined due to the slow inactivation process of the TTX-insensitive I_{Na} (see Figs 11 and 13).

To determine the forward and the backward rate constants for inactivation, a first-order kinetic model was applied as in the case of channel activation. The rate constants are shown in Fig. 12*C*. The forward rate constant (α_h) for the TTX-insensitive I_{Na} corresponding to the τ_h values at -30 to $+40$ mV potential range was not shown because at this potential range, α_h was nearly zero. The backward rate constant (β_h) for the TTX-sensitive I_{Na} was 3–7 times faster than that for the TTX-insensitive I_{Na} when values were compared in a comparable potential range (-10 to $+30$ mV). This indicates that the deactivation of the inactivation gate (h gate) is much faster than that for the TTX-insensitive I_{Na}.

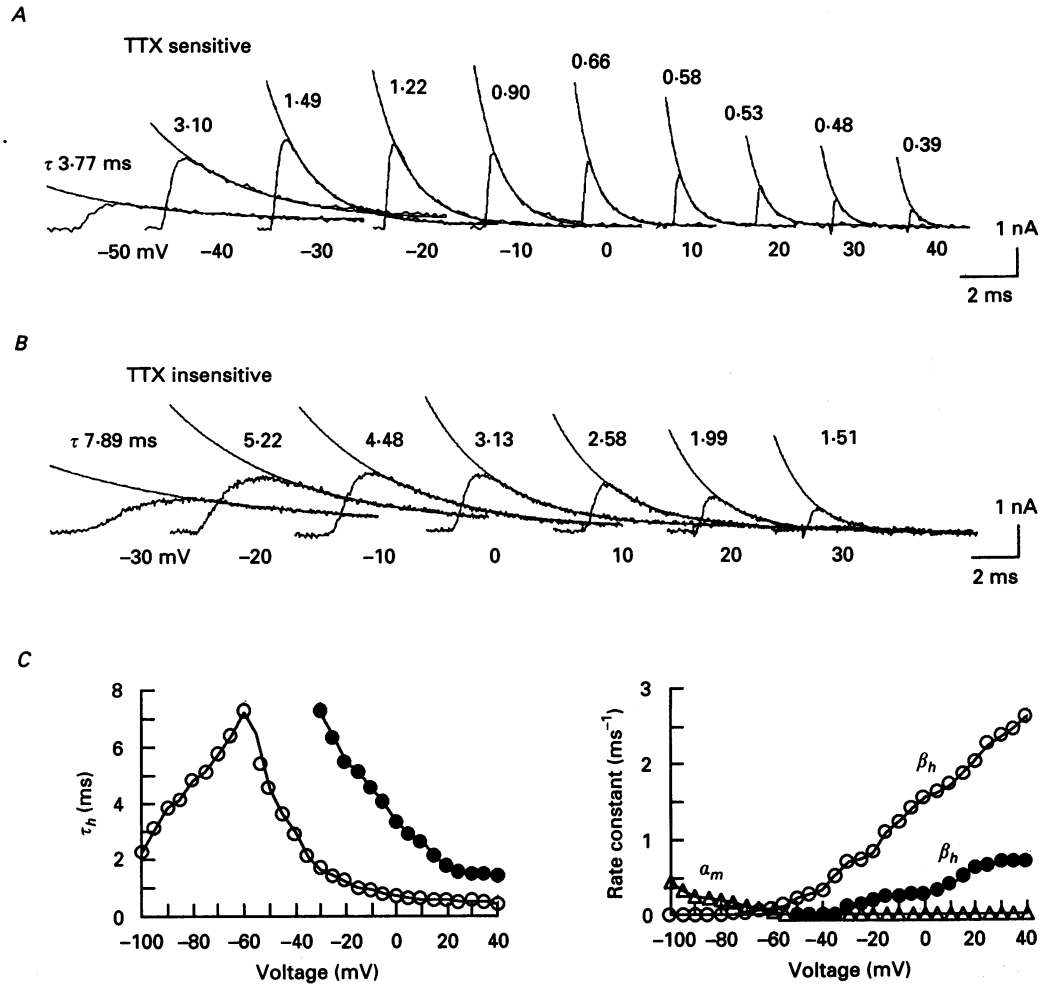

Fig. 12. Decay time course of the two types of I_{Na}. *A* and *B*, the decay phases of TTX-sensitive (*A*) and TTX-insensitive (*B*) I_{Na} evoked by step depolarizations to various potential levels were fitted by a single exponential function. *C*, the time constant of the exponential fit (τ_h) and the forward (α_h) and backward rate (β_h) constants for inactivation were plotted as a function of the test potential level. τ_h values for the TTX-sensitive I_{Na} at potentials positive to −55 mV were measured from the time constant (in ms) of the current decay. τ_h values for the TTX-sensitive I_{Na} at potentials negative to −60 mV were obtained from the fast component of the double exponential recovery process measured by a conventional double-pulse protocol. τ_h values for the TTX-insensitive I_{Na} at potentials positive to −30 mV were measured from the time constant of the current decay. α_h and β_h were calculated using the following equations:

$$\alpha_h = h_\infty/\tau_h; \quad \beta_h = (1-h_\infty)/\tau_h.$$

The values for h_{30} in Fig. 8*B* were used in place of h_∞ for the TTX-sensitive I_{Na}. The values for h_5 in Fig. 11*B* were used in place of h_∞ for the TTX-insensitive I_{Na}. *A*, TTX-sensitive cell: *B*, TTX-insensitive cell. In *C*, TTX-sensitive values represented by ○ and △; TTX-insensitive by ●.

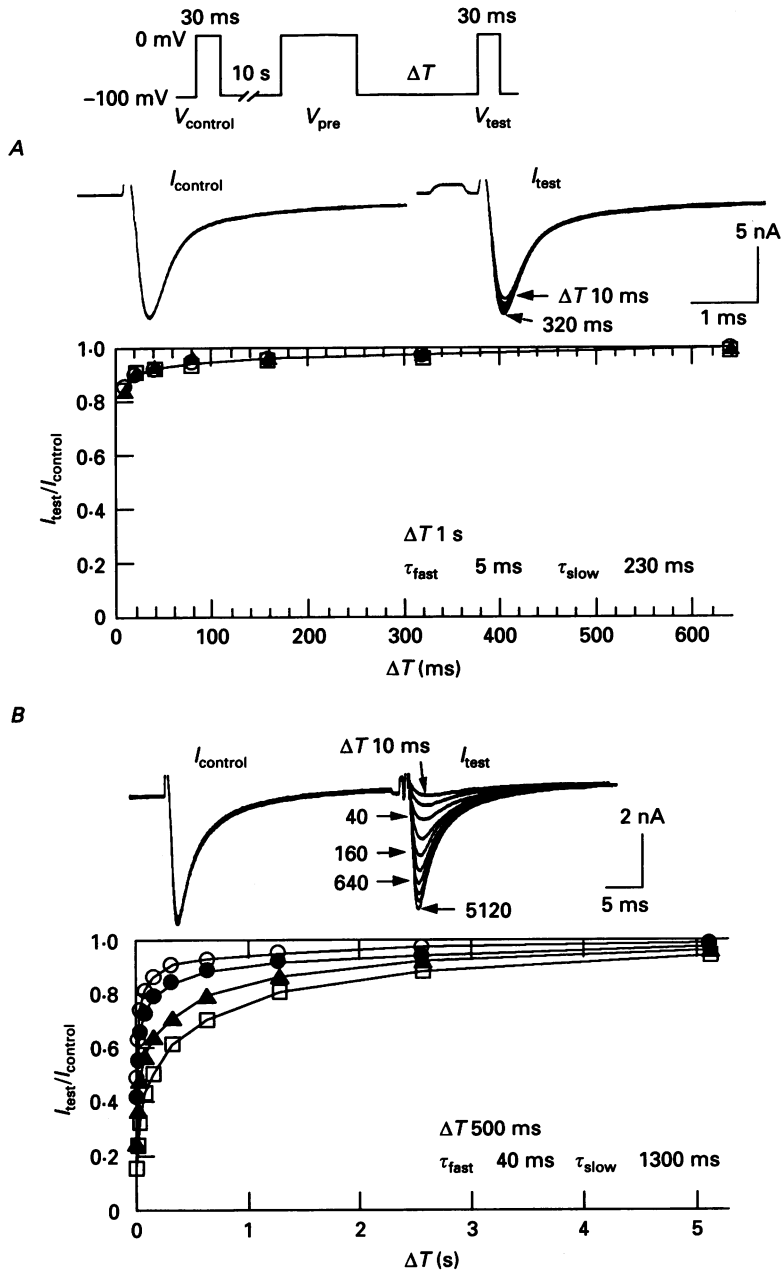

Fig. 13. Recovery from inactivation of the two types of I_{Na}. Inset illustrates experimental protocol. Two identical 30 ms step depolarizations to 0 mV were applied 10 s prior to ($V_{control}$) and ΔT (ms or s) after (V_{test}) the conditioning prepulse (V_{pre}) to 0 mV. The duration (ΔT) of V_{pre} was changed to various values. *A*, current traces in a TTX-sensitive cell evoked by $V_{control}$ ($I_{control}$) and by V_{test} (I_{test}) are shown superimposed. The value, $I_{test}/I_{control}$, was plotted as a function of ΔT. *B*, same as in *A* but in TTX-insensitive cell. In both *A* and *B*, continuous lines represent double exponential curves fitted to the data. Duration of V_{pre} represented by ○, 100 ms; ●, 200 ms; ■, 500 ms and □, 1 s.

Recovery from inactivation

Figure 13 illustrates the time dependence of the recovery from inactivation of TTX-sensitive and TTX-insensitive I_{Na}. The recovery from inactivation was fairly rapid in TTX-sensitive I_{Na} (Fig. 13*A*). The prepulse duration of 100 ms was sufficient to cause maximal inactivation, because the recovery time courses after prepulses of 0·1, 0·5 and 1 s were similar (see the graph in Fig. 13*A*). In contrast to the TTX-sensitive I_{Na}, the recovery from inactivation of TTX-insensitive I_{Na} was extremely slow, even after a relatively short prepulse (100 ms), and increased in parallel with the prepulse duration (Fig. 13*B*). The recovery process was described by two exponential functions in both the TTX-sensitive and TTX-insensitive I_{Na}. The fast and slow components of τ_h for the TTX-insensitive I_{Na} measured with a 500 ms prepulse were respectively about eight and six times larger than those of TTX-sensitive I_{Na}.

DISCUSSION

Present results show that DRG neurones have two types of Na^+ channels with different physiological and pharmacological properties. One type of Na^+ channel was activated at relatively negative membrane potentials and its activation and inactivation kinetics were relatively fast (thus, fast and low-threshold). This type of Na^+ channel was blocked by TTX in nanomolar concentrations. The other type was activated at more positive membrane potentials and had slow channel kinetics (thus, slow and high-threshold). This slow Na^+ channel was insensitive to a very high concentration (0·1 mM) of TTX.

Ionic dependence of the TTX-insensitive I_{Na}

The slow TTX-insensitive Na^+ channel is reminiscent of the Ca^{2+} channel in its insensitiveness to TTX and relatively slow time course of activation and inactivation. Since the TTX-insensitive I_{Na} was moderately inhibited by 2 mM Co^{2+} whereas the TTX-sensitive I_{Na} was not affected (Fig. 2*C* and *D*), the TTX-insensitive Na^+ channel may be phylogenetically closer to Ca^{2+} channels. Thus, it might be postulated that the TTX-insensitive inward current observed in this study was due to an influx of ions through Ca^{2+} channels. However, this possibility can be excluded from the following observations. (1) Fluorine ions, which are known to abolish Ca^{2+} channel currents, were used as the internal anion. (2) A high concentration of Cd^{2+} (50 μM), which totally blocks Ca^{2+} currents in rat DRG (Tatebayashi & Ogata, 1992), had no effect on this current. (3) The reversal potential for this current was dependent on the external concentration of Na^+ (Fig. 2*A*). (4) This current was not abolished in medium which was Ca^{2+}-free and contained 5 mM EGTA (Fig. 2*B*). Furthermore, the Ca^{2+} current observed in rat DRG had an activation threshold which was apparently more negative than the activation level of the TTX-insensitive I_{Na}, and the overall time course of the Ca^{2+} current was much longer than the TTX-insensitive I_{Na} (Ogata & Tatebayashi, 1992*b*).

TTX-insensitive Na^+ channel

Most of the voltage-gated Na^+ channels observed in cells from a variety of preparations are blocked by TTX (Narahashi, 1974). Several types of cells such as cardiac myocytes are somewhat resistant to TTX (Carmeliet, 1987*a*; Follmer *et al.* 1987). However, even in these cells, TTX in concentrations lower than 1 μM

TABLE 1. Kinetic parameters of two types of Na^+ channels

	TTX-sensitive Na^+ channel	TTX-insensitive Na^+ channel	
TTX-sensitivity (K_d, nM)	3·3	—	
I–V curve*			
Activation level (mV)	−56·9 ± 0·6	−36·2 ± 1·1	(n = 20)
Peak level (mV)	−29·2 ± 0·7	−0·6 ± 0·6	
m-parameter	3	1	
h-parameter	1	1	
τ_m (ms)			
at −30 mV	0·17 ± 0·01	0·7 ± 0·05	(n = 5)
at 0 mV	0·1 ± 0·01	0·48 ± 0·06	
τ_h (ms)			
at −30 mV	1·7 ± 0·09	7·5 ± 0·34	(n = 5)
at 0 mV	0·7 ± 0·07	3·4 ± 0·24	
Rate constants			
α_m (ms^{-1})			
at −30 mV	5·3	0·1	
at 0 mV	10·4	1·8	
β_m (ms^{-1})			
at −30 mV	0·72	1·3	
at 0 mV	0	0·3	
β_h (ms^{-1})			
at −30 mV	0·7	0·1	
at 0 mV	1·6	0·3	
m_∞			
$V_{\frac{1}{2}}$ (mV)	−41·6 ± 2·0	−16·0 ± 2·3	(n = 5)
slope factor (mV)	5·4 ± 0·7	5·8 ± 0·5	
h_∞†			
$V_{\frac{1}{2}}$ (mV)	−64·6 ± 0·8	−39·6 ± 0·8	(n = 5)
slope factor (mV)	5·1 ± 0·2	4·7 ± 0·3	
Current decay	Single exponential	Single exponential	
Recovery from inactivation (double pulse protocol)	Double exponential	Double exponential	
τ_{fast} (ms) at −80 mV	4·8 ± 0·6	42·5 ± 7·6	(n = 5)
τ_{slow} (ms) at −80 mV	223·5 ± 29·5	1350 ± 188	
Sensitivity to Cd^{2+} (50 μM)	—	—	
Sensitivity to Co^{2+} (2 mM)	—	30·2 ± 7·0 (% inhibition)	(n = 5)
Cell type‡	Large light cell	Small dark cell	
Diameter (μm)	39·4	20·5	

Values are means ± S.E.M.

* Measured in 1 mV step increments. † Measured with prepulses of 0·5 s duration. ‡ From Ogata & Tatebayashi (1991).

effectively blocked the Na^+ channel. In this respect, the TTX-insensitive Na^+ channel observed in sensory neurones is quite unique in that this type of channel was totally insensitive to TTX. We have shown that, in rat DRG, the TTX-insensitive Na^+ channels are already demonstrable at a very early stage of nervous system organogenesis (day seventeen of gestation) and are retained throughout the lifespan (Ogata & Tatebayashi, 1992*a*).

Although it has been reported that trypsin inhibits the action of TTX on Na^+ channels in *Helix* neurones (Lee, Akaike & Brown, 1977), the sensitivity of TTX-sensitive Na^+ channels in freshly dissociated DRG neurones to TTX was not affected (Ogata & Tatebayashi, 1992*a*). In addition, the preparation used in the present study was cultured cells. Thus, the insensitiveness of one type of the Na^+ channel to TTX was not due to enzymatic treatment.

TTX-insensitive Na^+ channels have been found in neurones of the spinal (Kostyuk *et al.* 1981; Ogata & Tatebayashi, 1992*a*) and cranial (Bossu & Feltz, 1984; Ikeda *et al.* 1986; Ikeda & Schofield, 1987) sensory ganglia, suggesting their role in the sensory integration. In addition, the TTX-insensitive channels may be involved in visceral sensation in the autonomic nervous system (Schofield & Ikeda, 1988; Groat *et al.* 1989; Clark *et al.* 1990). To our knowledge, TTX-insensitive Na^+ channels have not been reported in the central nervous system (Ogata & Tatebayashi, 1989; Ogata & Tatebayashi, 1990). It has been reported that the neurones in the substantia nigra (Guyenet & Aghajanian, 1978; Yung, Häusser & Jack, 1991) or in the ventral tegmental area (Yim & Mogenson, 1980; Wang, 1981) exhibit two types of action potentials with different durations. However, these neurones had a single type of TTX-sensitive Na^+ channel and the different durations of action potential were due to the differences in K^+ channel kinetics (H. Tatebayashi & N. Ogata, in preparation). Therefore, expression of the TTX-insensitive Na^+ appears to be a common feature of neurones in the peripheral nervous system.

Functional significance of the two types of Na^+ channels

Our results indicate that the gating kinetics of the two types of Na^+ channels with different affinities for TTX differ considerably. One of the most marked differences between Na^+ channels with different TTX-sensitivity was the rates of activation and inactivation of channels. The differences are summarized in Table 1. Although the TTX-sensitive Na^+ channel showed basically similar properties to Na^+ channels observed in other neuronal (e.g. Ogata & Tatebayashi, 1989; Ogata & Tatebayashi, 1990; Ogata *et al.* 1990) or non-neuronal (e.g. Ogata *et al.* 1989) preparations, properties of the TTX-insensitive Na^+ channel were quite exceptional in many respects. Therefore, the TTX-insensitive Na^+ channel appears to play a vital role in the processing of the primary sensory information.

Neurones in rat DRG have been divided into four groups based on the conduction velocity of their peripheral axons (Aα, 30–55 m s^{-1}; Aβ, 14–30 m s^{-1}; Aδ, 2·2–8 m s^{-1} and C < 1·4 m s^{-1}) (Harper & Lawson, 1985*a*). Harper & Lawson (1985*b*) found that the action potential observed in C fibre cells had a much slower time course than the action potential observed in A fibre cells. They also showed that the fast-conducting Aα and Aβ fibres had somata which fell within the size range of the large light cell population, while the size distribution of cells with slowly conducting C fibres

mimicked those of the small dark population, and it was not apparent to which of the populations the Aδ fibres belonged, since their mean cell size was intermediate between those of the large light and small dark cell populations. We have shown that the TTX-insensitive cells are preferentially found in the small dark cell population, while the TTX-sensitive cells are preferentially found in the large light cell population and that the size distribution of the partially TTX-sensitive cells was widely scattered covering the size ranges for the large light and small dark populations (Ogata & Tatebayashi, 1992*a*).

Due to different activation thresholds, the two types of Na^+ channels respond to depolarizing stimuli in a different manner. For example, when the membrane potential is sufficiently negative, a small depolarization (less than the threshold for the TTX-insensitive Na^+ channel of −40 mV) can only activate TTX-sensitive Na^+ channels, because this population is low-threshold. The TTX-insensitive Na^+ channels are excited only when sufficiently strong depolarizations are applied. Since the activation threshold of TTX-insensitive Na^+ channels overlaps with the negative slope region for activation of TTX-sensitive Na^+ channels (see current–voltage curve in Fig. 1*B* and *C*), TTX-sensitive Na^+ channels can provoke concomitant activation of TTX-insensitive Na^+ channels in cells where the two types of Na^+ channels co-exist. The different activation thresholds may be relevant to discrimination of different types of sensory signals.

The slow inactivation process characteristic of the TTX-insensitive Na^+ channels (see Fig. 11) appears to play an important role in the regulation of cellular long-term excitability. The inactivation curve obtained under steady-state conditions (5 min prepulse) showed a shift of approximately 20 mV towards negative potentials in comparison with the curve obtained using 1 s prepulses. This shift greatly reduced the overlap between the activation (m_∞) and inactivation curves (compare each inactivation curve with m_∞ in Fig. 11*B*). These results indicate that after approximately 5 min, no stationary inward current (window current) at membrane potentials between −40 and −20 mV can be expected. Such a reduction of the window current would cause a profound change in cellular excitability.

Since the two types of Na^+ channels examined in this study had different voltage- and time-dependent inactivation characteristics, the number of functional Na^+ channels, i.e. availability of Na^+ channel, could be modulated depending on the channel type and the membrane potential. A very important point is that the availability of only the TTX-sensitive Na^+ channels can be regulated by a prompt change of the membrane potential while the availability of the TTX-insensitive Na^+ channels is regulated by a long-term change of the membrane potential. For example, if we consider the situation where a membrane potential change lasting 0·5 s within a range of −80 to −50 mV occurs, the availability of the TTX-sensitive Na^+ channels can be effectively regulated by a change of the membrane potential because the inactivation of the TTX-sensitive Na^+ channels becomes steady state during this short period of potential change and the inactivation curve at this potential range is steeply voltage dependent (see Fig. 8*B*). On the contrary, a comparable membrane potential change can affect only a small portion of the TTX-insensitive Na^+ channels, because the availability of TTX-insensitive Na^+ channels in such a situation is nearly maximal (see Fig. 9*B*).

With a prolonged membrane potential shift of the order of minutes, the inactivation curve for the TTX-insensitive Na^+ channels becomes similar to the inactivation curve for the TTX-insensitive Na^+ channels (compare the h_∞ curve in Fig. 8*B* with the inactivation curve for 5 min prepulse in Fig. 11*B*). Thus, the availability of TTX-insensitive Na^+ channel can only be modified after a prolonged change (of the order of minutes) of the membrane potential. Therefore, it might be assumed that the TTX-sensitive Na^+ channel is suitable for signals which need to be constantly adapted while the TTX-insensitive Na^+ channel is suitable for signals which need to be maintained at a relatively stable level.

The recovery process from inactivation was markedly slow in the TTX-insensitive Na^+ channels, whereas the recovery process in the TTX-sensitive Na^+ channels was rapid (Fig. 13). TTX-insensitive Na^+ channels would fail to respond to repeated membrane depolarizations. Therefore, only a limited frequency of signals could be processed by the TTX-insensitive action potential. The slow recovery process of the TTX-insensitive Na^+ channel may also be related to adaptation, a phenomenon commonly observed in sensation.

In conclusion, action potential generation in rat DRG appears to be controlled depending on the availabilities of two distinct types of Na^+ channels which are modulated in time- and voltage-dependent manner by a preceding history of membrane potential change.

We thank Professor H. Kuriyama for his support and advice, and Dr M. Yoshii for helpful discussions. This study was supported by the Japanese Ministry of Education (Scientific Research 63570096).

REFERENCES

Bossu, J. L. & Feltz, A. (1984). Patch-clamp study of the tetrodotoxin-resistant sodium current in group C sensory neurons. *Neuroscience Letters* **51**, 241–246.

Carmeliet, E. (1987*a*). Voltage-dependent block by tetrodotoxin of the sodium channel in rabbit cardiac Purkinje fibres. *Biophysical Journal* **51**, 109–114.

Carmeliet, E. (1987*b*). Slow inactivation of the sodium current in rabbit cardiac Purkinje fibers. *Pflügers Archiv* **408**, 18–26.

Chandler, W. K. & Meves, H. (1970). Rate constants associated with changes in sodium conductance in axons perfused with sodium fluoride. *Journal of Physiology* **211**, 679–705.

Chiu, S. Y. (1977). Inactivation of sodium channels: second order kinetics in myelinated nerve. *Journal of Physiology* **273**, 573–596.

Clark, R. B., Tse, A. & Giles, W. R. (1990). Electrophysiology of parasympathetic neurones isolated from the interatrial septum of bull-frog heart. *Journal of Physiology* **427**, 89–125.

Cohen, C. J., Bean, B. P., Colatsky, T. J. & Tsien, R. W. (1981). Tetrodotoxin block of sodium channels in rabbit Purkinje fibers. *Journal of General Physiology* **78**, 383–411.

Colquhoun, D. & Ritchie, J. M. (1972). The kinetics of the interaction between tetrodotoxin and mammalian nonmyelinated nerve fibers. *Molecular Pharmacology* **8**, 285–292.

Cuervo, L. A. & Adelman, W. J. Jr (1970). Equilibrium and kinetic properties of the interaction between tetrodotoxin and the excitable membrane of the squid giant axon. *Journal of General Physiology* **55**, 309–335.

Follmer, C. H., Ten Eick, R. E. & Yeh, J. Z. (1987). Sodium current kinetics in cat myocytes. *Journal of Physiology* **384**, 169–197.

Fox, J. M. (1976). Ultra-slow inactivation of the ionic currents through the membrane of myelinated nerve. *Biochimica et Biophysica Acta* **426**, 232–244.

FRANKENHAEUSER, B. & HODGKIN, A. L. (1957). The action of calcium on the electrical properties of squid axons. *Journal of Physiology* **137**, 217–244.

FUKUDA, J. & KAMEYAMA, M. (1980). Tetrodotoxin-sensitive and tetrodotoxin-resistant sodium channels in tissue-cultured spinal ganglion neurons from adult mammals. *Brain Research* **182**, 191–197.

GILLESPIE, J. I. & MEVES, H. (1981). The effect of external potassium on the removal of sodium inactivation in squid giant axons. *Journal of Physiology* **315**, 493–514.

GROAT, W. C., WEIGHT, F. F. & WHITE, G. (1989). A patch-clamp analysis of tetrodotoxin (TTX)-sensitive and resistant Na^+ currents in neurons isolated from sensory and parasympathetic ganglia of the adult rat. *Neuroscience Abstracts* **15**, 440.

GUYENET, P. G. & AGHAJANIAN, G. K. (1978). Antidromic identification of dopaminergic and other output neurons of the rat substantia nigra. *Brain Research* **150**, 69–84.

HAMILL, O. P., MARTY, A., NEHER, E., SAKMANN, B. & SIGWORTH, F. J. (1981). Improved patch-clamp techniques for high-resolution current recording from cells and cell-free membrane patches. *Pflügers Archiv* **391**, 85–100.

HARPER, A. A. & LAWSON, S. N. (1985*a*). Conduction velocity is related to morphological cell type in rat dorsal root ganglion neurons. *Journal of Physiology* **359**, 31–46.

HARPER, A. A. & LAWSON, S. N. (1985*b*). Electrical properties of rat dorsal root ganglion neurones with different peripheral nerve conduction velocities. *Journal of Physiology* **359**, 47–63.

HODGKIN, A. L. & HUXLEY, A. F. (1952). A quantitative description of membrane current and its application to conduction and excitation in nerve. *Journal of Physiology* **117**, 500–544.

IKEDA, S. R. & SCHOFIELD, G. G. (1987). Tetrodotoxin-resistant sodium current of rat nodose neurones: monovalent cation selectivity and divalent cation block. *Journal of Physiology* **389**, 255–270.

IKEDA, S. R., SCHOFIELD, G. G. & WEIGHT, F. F. (1986). Na^+ and Ca^{2+} currents of acutely isolated adult rat nodose ganglion cells. *Journal of Neurophysiology* **55**, 527–539.

JACK, J. J. B., NOBLE, D. & TSIEN, R. W. (1983). *Electric Current Flow in Excitable Cells*. Clarendon Press, Oxford.

KOSTYUK, P. G., VESELOVSKY, S. & TSYNDRENKO, A. Y. (1981). Ionic currents in the somatic membrane of rat dorsal root ganglion neurones. I. Sodium currents. *Neuroscience* **6**, 2423–2430.

LAWSON, S. N., HARPER, A. A., HARPER, E. I., GARSON, J. A. & ANDERTON, B. H. (1984). A monoclonal antibody against neurofilament protein specifically labels a subpopulation of rat sensory neurones. *Journal of Comparative Neurology* **228**, 263–272.

LEE, K. S., AKAIKE, N. & BROWN, A. M. (1977). Trypsin inhibits the action of tetrodotoxin on neurones. *Nature* **265**, 751–753.

LEE, K. H., CHUNG, K., CHUNG, J. M. & COGGESHALL, R. E. (1986). Correlation of cell body size, axon size, and signal conduction velocity for individually labelled dorsal root ganglion cells in the cat. *Journal of Comparative Neurology* **243**, 335–346.

NARAHASHI, T. (1974). Chemicals as tools in the study of excitable membranes. *Physiological Review* **54**, 813–889.

NARAHASHI, T., TSUNOO, A. & YOSHII, M. (1987). Characterization of two types of calcium channels in mouse neuroblastoma cells. *Journal of Physiology* **383**, 231–249.

OGATA, N., NISHIMURA, M. & NARAHASHI, T. (1989). Kinetics of blocking action of psychotropic drugs on sodium channels in single guinea pig ventricular myocytes. *Journal of Pharmacology and Experimental Therapeutics* **248**, 605–613.

OGATA, N. & TATEBAYASHI, H. (1989). Modulation of sodium current kinetics by chlorpromazine in freshly-isolated striatal neurones of the adult guinea-pig. *British Journal of Pharmacology* **98**, 1173–1184.

OGATA, N. & TATEBAYASHI, H. (1990). Sodium current kinetics in freshly isolated neostriatal neurones of the adult guinea pig. *Pflügers Archiv* **416**, 594–603.

OGATA, N. & TATEBAYASHI, H. (1991). A simple and multi-purpose 'concentration-clamp' method for rapid superfusion. *Journal of Neuroscience Methods* **39**, 175–183.

OGATA, N. & TATEBAYASHI, H. (1992*a*). Ontogenic development of the TTX-sensitive and TTX-insensitive Na^+ channels in neurons of the rat dorsal root ganglia. *Developmental Brain Research* **65**, 93–100.

OGATA, N. & TATEBAYASHI, H. (1992*b*). Comparison of two types of Na^+ currents with low-voltage-activated T-type Ca^{2+} current in newborn rat dorsal root ganglia. *Pflügers Archiv* **420**, 590–594.

OGATA, N., YOSHII, M. & NARAHASHI, T. (1990). Differential block of sodium and calcium channels by chlorpromazine in mouse neuroblastoma cells. *Journal of Physiology* **420**, 165–183.

PATLAK, J. B. & ORTIZ, M. (1985). Slow currents through single Na^+ channels of the adult rat heart. *Journal of General Physiology* **86**, 89–104.

QUANDT, F. N., YEH, J. Z. & NARAHASHI, T. (1985). All or none block of single Na^+ channels by tetrodotoxin. *Neuroscience Letters* **54**, 77–83.

SCHOFIELD, G. G. & IKEDA, S. R. (1988). Sodium and calcium currents of acutely isolated adult rat superior cervical ganglion neurons. *Pflügers Archiv* **411**, 481–490.

SCHOUTEN, V. J. A. & MORAD, M. (1989). Regulation of Ca^{2+} current in frog ventricular myocytes by the holding potential, c-AMP and frequency. *Pflügers Archiv* **415**, 1–11.

TATEBAYASHI, H. & OGATA, N. (1992). Kinetic analysis of the $GABA_B$-mediated inhibition of the high-threshold Ca^{2+} current in cultured rat sensory neurones. *Journal of Physiology* **447**, 391–407.

WANG, R. Y. (1981). Dopaminergic neurons in the rat ventral tegmental area. I. Identification and characterization. *Brain Research Reviews* **3**, 123–140.

YIM, C. Y. & MOGENSON, G. J. (1980). Electrophysiological studies of neurons in the ventral tegmental area of Tsai. *Brain Research* **181**, 301–313.

YOSHIDA, S., MATSUDA, Y. & SAMEJIMA, A. (1978). Tetrodotoxin-resistant sodium and calcium components of action potentials in dorsal root ganglion cells of the adult mouse. *Journal of Neurophysiology* **41**, 1096–1106.

YUNG, W. H., HÄUSSER, M. A. & JACK, J. J. B. (1991). Electrophysiology of dopaminergic and non-dopaminergic neurones of the guinea-pig substantia nigra pars compacta *in vitro*. *Journal of Physiology* **436**, 643–667.